

THE OXYGEN ABUNDANCES OF LUMINOUS AND ULTRALUMINOUS INFRARED GALAXIES

DAVID S. N. RUPKE, SYLVAIN VEILLEUX

Department of Astronomy, University of Maryland, College Park, MD 20742-2421

AND ANDREW J. BAKER

Department of Physics and Astronomy, Rutgers, the State University of New Jersey, 136 Frelinghuysen Road, Piscataway, NJ 08854-8019

Draft version November 8, 2018

ABSTRACT

Luminous and ultraluminous infrared galaxies (LIRGs and ULIRGs) dominate the star formation rate budget of the universe at $z \gtrsim 1$, yet no local measurements of their heavy element abundances exist. We measure nuclear or near-nuclear oxygen abundances in a sample of 100 star-forming LIRGs and ULIRGs using new, previously published, and archival spectroscopy of strong emission lines (including [O II] $\lambda\lambda 3727, 3729$) in galaxies with redshifts $\langle z \rangle \sim 0.1$. When compared to local emission-line galaxies of similar luminosity and mass (using the near-infrared luminosity-metallicity and mass-metallicity relations), we find that LIRGs and ULIRGs are under-abundant by a factor of two on average. As a corollary, LIRGs and ULIRGs also have smaller effective yields. We conclude that the observed under-abundance results from the combination of a decrease of abundance with increasing radius in the progenitor galaxies and strong, interaction- or merger-induced gas inflow into the galaxy nucleus. This conclusion demonstrates that local abundance scaling relations are not universal, a fact that must be accounted for when interpreting abundances earlier in the universe's history when merger-induced star formation was the dominant mode. We use our local sample to compare to high-redshift samples and assess abundance evolution in LIRGs and ULIRGs. We find that abundances in these systems increased by ~ 0.2 dex from $z \sim 0.6$ to $z \sim 0.1$. Evolution from $z \sim 2$ submillimeter galaxies to $z \sim 0.1$ ULIRGs also appears to be present, though uncertainty due to spectroscopic limitations is large.

Subject headings: galaxies: abundances — galaxies: evolution — galaxies: interactions — galaxies: ISM — galaxies: kinematics and dynamics — infrared: galaxies

1. INTRODUCTION

Mid-infrared and submillimeter observations show that luminous and ultraluminous infrared galaxies (LIRGs and ULIRGs)¹ host most of the star formation in the universe at $z \gtrsim 1$ (Le Floc'h et al. 2005; Chapman et al. 2005; Daddi et al. 2005; Wang et al. 2006; Caputi et al. 2007). Understanding local examples of these sources is thus a window to star formation and accretion onto supermassive black holes at the epoch of highest star formation rate and active galactic nucleus (AGN) density (e.g., Madau et al. 1998; Schmidt et al. 1995).

A great deal is known about nearby ULIRGs; for a recent review see Lonsdale et al. (2006). All ULIRGs possess strong starbursts, and many also host optically-visible AGN (Veilleux et al. 1999). The starbursts and AGN are on average heavily obscured (Genzel et al. 1998; Hao et al. 2007), and optically-invisible AGN may be present (Lutz et al. 1999; Armus et al. 2007). The prevalence of optically-visible AGN increases with increasing infrared luminosity (Veilleux et al. 1999) and as the merger progresses (Veilleux et al. 2002). It is thus hypothesized that ULIRGs play a role in the evolution of quasars. When obscuring dust is removed from a buried AGN (by starburst- or AGN-driven outflows; see, e.g., Rupke et al. 2005a,c), a bright

quasar is left (Sanders et al. 1988). This hypothesis is under scrutiny; comparison to the fundamental plane of ellipticals shows that many ULIRGs are evolving into moderate-mass ellipticals (Genzel et al. 2001; Veilleux et al. 2002; Tacconi et al. 2002; Dasyra et al. 2006a,b), similar to but slightly less massive than the hosts of optically bright quasars (Dasyra et al. 2007).

LIRGs host less intense starbursts than ULIRGs, and the frequency of occurrence of optically-visible AGN in LIRGs is much smaller (Veilleux et al. 1995). Photometric studies divide LIRGs into two groups (Ishida 2004). The most luminous are early in the merger sequence of two roughly equal-mass galaxies, and thus may be the progenitors of ULIRGs (Arribas et al. 2004; Ishida 2004). Other LIRGs are unequal-mass mergers or isolated disk galaxies which may or may not be experiencing an interaction (Ishida 2004). Kinematic studies confirm that the pair mass ratios in at least some LIRG interactions are of order 1 – 3 (Rothberg & Joseph 2006; Dasyra et al. 2006a).

The interstellar medium in LIRGs and ULIRGs is in a kinematically extreme state, dominated by inflows (e.g., Barnes & Hernquist 1996; Mihos & Hernquist 1996), outflows (Heckman et al. 2000; Rupke et al. 2002, 2005a,b,c; Martin 2005, 2006; see Veilleux et al. 2005 for a recent review), and turbulent motions (Downes & Solomon 1998). These gas motions have the power to significantly alter the chemical states of the progenitor galaxies (e.g., Edmunds 1990; Köppen & Edmunds 1999; Dalcanton 2007). Ongoing,

Electronic address: drupke@astro.umd.edu

¹ LIRGs are defined by $10^{11} < L_{\text{IR}}/L_{\odot} < 10^{12}$ and ULIRGs by $10^{12} < L_{\text{IR}}/L_{\odot} < 10^{13}$, where L_{IR} is the 'total' infrared luminosity from 8 – 1000 μm .

intense star formation in LIRGs and ULIRGs is also producing and redistributing heavy metals at a prodigious rate. In this paper we describe the first comprehensive study of the oxygen abundances of local LIRGs and ULIRGs (§§2 – 3). This will allow us to assess the effects of these processes on the gas-phase abundances of infrared-selected, interacting galaxies. Studies of optically-selected mergers suggest that gas motions do alter nuclear abundances (Kewley et al. 2006a). Here we present evidence that this is true also of strong mergers with high star formation rates.

In order to understand the chemical evolution of LIRGs and ULIRGs, it is crucial to compare these sources to weakly- or non-interacting galaxies with modest star formation, which represent the progenitors of LIRGs and ULIRGs. To this end, we compare LIRGs and ULIRGs to published luminosity-metallicity, mass-metallicity, and mass-effective yield relations (§§4 – 6). We discuss these results in §7.

There exist a few measurements of oxygen abundances in high-redshift infrared-luminous galaxies. Liang et al. (2004) measure the abundances of ~ 20 $z = 0.4 – 0.9$ LIRGs selected at $15 \mu\text{m}$ by the *Infrared Space Observatory (ISO)*. Abundance measurements also exist for a handful of $z \sim 2$ submillimeter-selected galaxies that have total infrared luminosities greater than or equal to those of ULIRGs (Tecza et al. 2004; Swinbank et al. 2004). Finally, we describe in this paper a handful of new moderate-redshift measurements.

While these high- z measurements are valuable on their own, they are also sparse and, in many cases, uncertain. The more robust measurements of local LIRGs and ULIRGs that we report here facilitate two comparisons: we can now compare the enrichment histories of infrared-luminous and infrared-faint galaxies in the local universe (§§ 4.2, 4.3, and 5); and we can look for evidence of chemical evolution among infrared-luminous populations as a function of redshift (§4.4).

We summarize our work and discuss its consequences in §8.

Throughout the paper, we use the notation (O/H) to refer to the ratio of the number densities of O and H atoms in the ISM. The variable Z refers instead to the mass fraction of O relative to the total mass of gas. These two variables are related by a constant: $Z = 16/C(\text{O}/\text{H})$, where $C \sim 1.4$ is the ratio of total to H gas masses. Where appropriate, we use (O/H) and Z interchangeably. For the solar oxygen abundance, we use the recent value from Asplund et al. (2004): $12 + \log(\text{O}/\text{H})_{\odot} = 8.66$. For all calculations, we assume the standard cosmology of $H_0 = 75 \text{ km s}^{-1} \text{ Mpc}^{-1}$, $\Omega_m = 0.3$, and $\Omega_{\Lambda} = 0.7$.

2. SAMPLE SELECTION

Abundance diagnostics of star-forming galaxies rely mostly on emission lines. The emission lines of many LIRGs and ULIRGs, however, may include contributions from an AGN and/or strong shocks (Kim et al. 1998; Veilleux et al. 1999). Abundance diagnostics are generally calibrated using galaxies with modest star formation, whose emission line fluxes do not contain strong contributions from either of these ionization mechanisms. Thus, choosing galaxies whose lines are starburst-dominated is important for computing accurate abundances.

This decision is complicated by the multiple options

for defining a star-forming galaxy in the phase space of optical emission line flux ratios. For instance, using the classic diagnostics of Veilleux & Osterbrock (1987), 60% of LIRGs and one-third of all ULIRGs are ‘H II-region-like’ galaxies (Veilleux et al. 1995, 1999). More recent work updates this empirical classification scheme using $\sim 10^5$ galaxies from the Sloan Digital Sky Survey (SDSS; Kauffmann et al. 2003; Kewley et al. 2006b). Many LIRGs and ULIRGs classified as H II galaxies using the Veilleux & Osterbrock (1987) scheme lie away from the bulk of local star-forming galaxies; instead, they lie in the region of the $[\text{O III}]\lambda 5007/\text{H}\beta$ vs. $[\text{N II}]\lambda 6583/\text{H}\alpha$ flux ratio diagram that is between the outer boundary of the locus of SDSS galaxies (Kauffmann et al. 2003) and the line delineating the maximum line ratios achievable by starbursts, according to theory (Kewley et al. 2001).

In §3.3, we discuss in detail the abundance uncertainties that arise from such physical effects. For now, we adopt loose initial selection criteria. We include in our sample all galaxies classified as H II galaxies or low ionization nuclear emission-line regions (LINERs) under any scheme. We also require that line flux uncertainties be smaller than 50%; almost all fluxes are far more certain than this, but a few fall near the limit. In Figure 1, we place the galaxies in the current sample on several line-ratio diagrams, with various classification schemes over-plotted.

Our ULIRGs are primarily from the 1 Jy sample, which is a complete, flux-limited, northern-hemisphere sample drawn from the *Infrared Astronomical Satellite (IRAS)* database (Kim & Sanders 1998). We require that our galaxies have measured $[\text{O II}]\lambda\lambda 3727, 3729$ fluxes. The moderately-high-resolution spectra of Rupke et al. (2002, 2005b), from Keck or the MMT, have broad enough wavelength coverage for this purpose. We supplement this data set with a handful of spectra of 1 Jy objects from the Fifth Data Release of the SDSS (York et al. 2000; Strauss et al. 2002; Adelman-McCarthy et al. 2007). To improve our statistics, we also include a few ULIRGs with published $[\text{O II}]$ fluxes from the Revised Bright Galaxy Sample (RBGS), the Warm Galaxy Survey (WGS), and the 2 Jy survey (Kim et al. 1995; Wu et al. 1998). The final local sample of 31 galaxy nuclei has $\langle z \rangle = 0.14$, with a maximum redshift of 0.27. However, in addition we include measurements for a few galaxies with $z = 0.4 – 0.5$ from the FIRST-FSC catalog (Stanford et al. 2000; Rupke et al. 2005b) for the purpose of assessing redshift evolution (§4.4).

We have selected our LIRGs primarily from the Revised Bright Galaxy Sample, which is also a complete, flux-limited *IRAS* sample (Sanders et al. 2003). Our RBGS data come from a variety of spectroscopic surveys: (1) Kim et al. (1995); (2) Liu & Kennicutt (1995); (3) Wu et al. (1998); (4) Rupke et al. (2002, 2005c); (5) the Fourth Data Release of the SDSS (Adelman-McCarthy et al. 2006); and (6) Moustakas & Kennicutt (2006, nuclear spectra only). Again, to improve our statistics, we include published fluxes of galaxies from the Warm Galaxy Survey (WGS) and 2 Jy sample (Kim et al. 1995; Wu et al. 1998). The sample of 65 galaxy nuclei has $\langle z \rangle = 0.04$. (We also have measurements for one LIRG with $z = 0.48$, which we use in §4.4.)

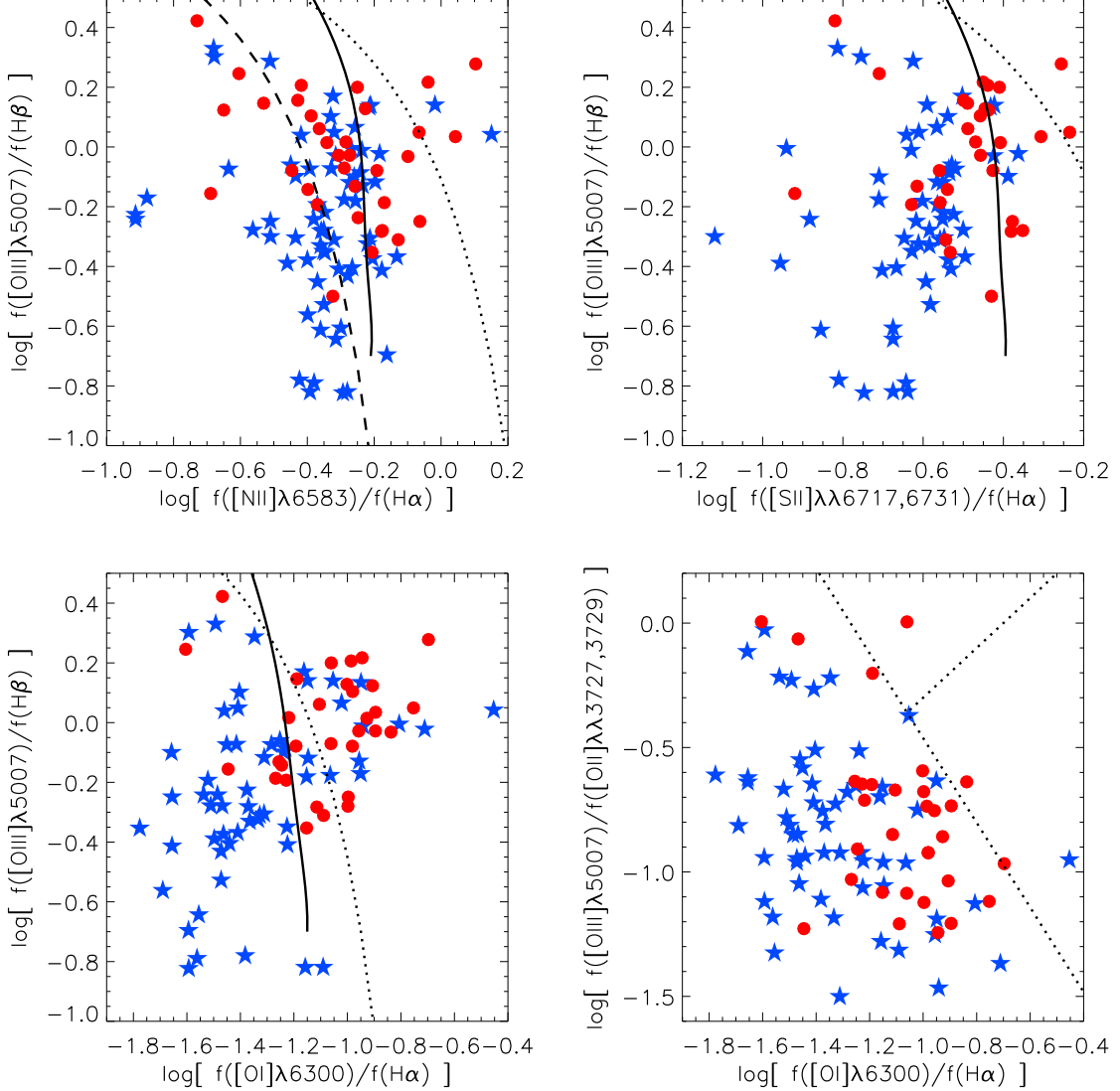


FIG. 1.— Emission-line ratio diagrams, with fluxes corrected for extinction. Blue stars are luminous infrared galaxies and red circles are ultraluminous infrared galaxies. The solid lines separate star-forming galaxies from LINERs (Veilleux & Osterbrock 1987); the dotted lines denote the phase space limits of the Kewley et al. (2001) starburst models in all plots except the bottom right, where they separate starbursts, LINERs, and AGN (Kewley et al. 2006b); and the dashed line denotes the outer boundary of the bulk of star-forming galaxies in the SDSS (Kauffmann et al. 2003).

The selected galaxies are representative of the local ($z \lesssim 0.2$), star-forming, infrared-luminous galaxy population. The 1 Jy sample, 2 Jy sample, RBGS, WGS are complete samples. The particular galaxies which appear in this paper are effectively a random selection from these samples, since they are culled from their parent spectroscopic studies only on the basis of spectral type and signal-to-noise ratio. The parent studies from which our spectroscopic data were collated impose various constraints on sky location, emission-line sensitivity, and (to a minor degree) redshift. However, these have no effect on the physical properties of the galaxies chosen, as shown by comparisons among Figure 1 and similar figures from the parent studies (e.g., Kim et al. 1995; Veilleux et al. 1999).

Some of the galaxies in our sample are multiple-nucleus

systems². For the 1 Jy ULIRGs, the nuclei are characterized using sensitive optical and near-infrared imaging (Kim et al. 2002; Veilleux et al. 2002). For other sources, we specify nuclei using unique designations from the NASA/IPAC Extragalactic Database (NED; see Table 1). We treat each nucleus separately in our analysis, since the apertures for our spectra are nuclear or near-nuclear (§3.3). Accordingly, for each multiple-nucleus system we divide the total system infrared luminosity between component nuclei based on resolved *IRAS* imaging (Surace et al. 2004) or the near-infrared luminosities of the component galaxies (§4.1). The fraction of the total infrared luminosity of the system belonging to each nucleus (or equivalently fractional near-infrared luminos-

² For some multiple-nucleus systems, only one nucleus enters our sample. This is due to a lack of data or because the other nucleus has a Seyfert optical spectral type.

ity) for those systems where the NIR luminosity is used to divide L_{IR} is listed in Table 1. Seven ULIRG nuclei descend into the LIRG category due to their nuclear luminosity. This reclassification does not impact our results.

In total, there are 100 galaxies or nuclei in our sample. Table 1 lists the basic properties of each galaxy or nucleus.

The strong emission lines in the Rupke et al. (2002, 2005b) and SDSS flux-calibrated spectra were measured using the IRAF task SPLOT. The average measurement uncertainty in the brightest lines (e.g., [O II] or [N II]) is 5% or less. For weak or noisy lines ([O I], [O III], or [S II] in a few cases) or those affected by a continuum that has strong stellar absorption, the uncertainty rises to $\sim 20 - 30\%$. Table 2 lists the line fluxes newly measured for this study.

Our Keck, MMT, and SDSS spectra are typically of high enough resolution for us to fit simultaneously a Voigt absorption and Gaussian emission component to H β . In the few cases where this was not possible, we used lower order Balmer lines to estimate the expected absorption in H β . We corrected the H α emission line in these galaxies for stellar absorption by extrapolating from the absorption equivalent widths of lower order Balmer lines, using the relative values for different lines predicted by the oscillator strengths (Menzel 1969):

$$W_{eq}(\text{H}\alpha) = \frac{W_{eq}(\text{H}_N)}{\sum_{i=3}^N f(\text{H}_i)}. \quad (1)$$

In this equation, H $_N$ is the Balmer transition from which the equivalent width of H α is to be calculated; H $_i$ represents the Balmer transition with upper principal quantum number i (e.g., H $_4$ = H β); and $f(\text{H}_i)$ is its oscillator strength. Patris et al. (2003) tabulate the coefficient values that we used. Table 2 lists the (absorption-uncorrected) H α emission line and H β absorption line equivalent widths for newly measured data.

The emission lines were corrected for extinction using the Balmer decrement. We assume an intrinsic H α /H β flux ratio of 2.86 (Hummer & Storey 1987), an effective foreground screen, and the starburst attenuation curve of Calzetti et al. (2000). Table 2 lists the E(B-V) values for newly measured data.

The data quality was checked through cross-correlation of objects common to different data sets. The results showed remarkable consistency, given the number of references from which the data were drawn. The typical discrepancy between two measurements of the same galaxy nucleus is of the order ~ 0.1 dex. Where multiple data were available for a given source, we chose the spectrum with highest spectral resolution and signal-to-noise. Exceptions are sources not drawn from the 1 Jy sample or RBGS that have both published and SDSS spectra; for consistency, we chose the published data even though the SDSS data may be of higher spectral resolution or sensitivity. We decided to use the SDSS data only to supplement the number of spectra available from the 1 Jy sample and RBGS (or for data quality checking) in order to keep the sample selection fairly clean and the size of the sample manageable. (I.e., there are a large number of infrared-luminous galaxies in the SDSS that we did not include; e.g., Pasquali et al. 2005.)

3. ABUNDANCES

3.1. Comparison of Diagnostics

Numerous strong-line abundance diagnostics exist, each relying on different combinations of the strongest emission lines measurable in optical spectra. Each diagnostic in turn has different absolute calibrations, based on photoionization models, electron temperature (T_e) measurements (i.e., weak-line diagnostics), or a combination of the two. Different diagnostics, or different calibrations of the same diagnostic, can give vastly different abundances for the same galaxy or group of galaxies. For instance, models calibrated on measurements of electron temperatures of H II regions in nearby galaxies differ from theoretical calibrations by factors of a few (see, e.g., Kennicutt et al. 2003, and references therein).

To help the reader understand the uncertainty that attaches to the choice of a particular diagnostic/calibration combination, we have investigated several different options. One of these (the Tremonti et al. 2004 calibration) we employ in §§ 4–6 to compare our data with published luminosity-metallicity ($L - Z$), mass-metallicity ($M - Z$), and mass-effective yield relations. The others provide a useful baseline comparison and illustrate some of the uncertainties due to choice of calibration and physical effects.

1. Pilyugin & Thuan (2005) collate recent T_e measurements and use them to calibrate simultaneous fits to $R_{23} \equiv \{f(\text{[O II]}) + f(\text{[O III]}\lambda\lambda 4959, 5007)\}/f(\text{H}\beta)$ and a function of $O_{32} \equiv f(\text{[O III]}\lambda\lambda 4959, 5007)/f(\text{[O II]})$. The latter is a proxy for ionization parameter, which is the ratio of ionizing photons to hydrogen nuclei present in gas.
2. The photoionization models of McGaugh (1991) also use both R_{23} and O_{32} as parameters in the diagnostic. The calibration is updated and printed in analytic form by Kuzio de Naray et al. (2004); we use their semi-empirical version.
3. Tremonti et al. (2004, hereafter T04) use the models of Charlot & Longhetti (2001, hereafter CL01) to compute the abundances of $\sim 10^5$ galaxies from the SDSS. The original models are a suite of analytic functions involving different combinations of strong emission lines; the choice of diagnostic then depends on the spectral data available. However, T04 directly cross-correlate their data with model spectra to find the best-fit abundance. They then fit a simple analytic function to the upper branch of the abundance vs. R_{23} relation.
4. For comparison with the T04 R_{23} calibration, we include the original CL01 suite of analytic functions. We compute abundances using the diagnostics of Cases A through F, where successive diagnostic cases rely on less spectral information than the previous one. For simplicity, we only discuss Cases A and F to represent the range of possibilities in spectral information. The former relies on $[\text{N II}]\lambda 6583/[\text{S II}]\lambda\lambda 6717, 6731$ and the latter on $[\text{O III}]\lambda 5007/\text{H}\beta$ (with O_{32} as a weak secondary parameter in each case). We note that the CL01 diagnostics use observed fluxes as inputs, unlike most

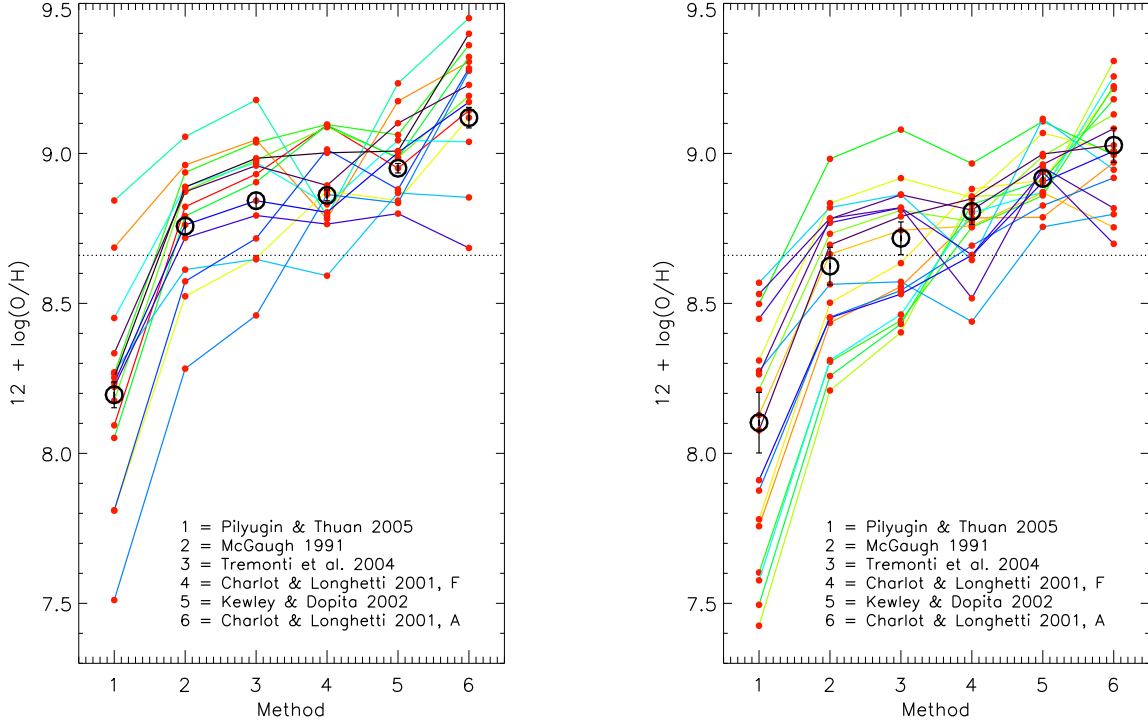


FIG. 2.— Abundances in six different diagnostic/calibration systems. (See §3.1 for a description of each system.) We select a random sample of LIRGs (left) and ULIRGs (right). Colored lines connect different calibrations for the same galaxy. The heavy open circles and error bars reflect the median and standard error over the entire sample in each system. We here consider only galaxies that pass the second emission-line cut (§3.3).

other diagnostics which use fluxes corrected for attenuation by dust.

5. Kewley & Dopita (2002) attempt an optimal calibration by comparing their photoionization models to previous work and combining several diagnostics. For our galaxies, their ‘combined’ diagnostic reduces to the $[\text{N II}]\lambda 6583/[\text{O II}]\lambda\lambda 3727, 3729$ diagnostic in almost all cases.

In each case, we discard galaxies that have $\log(R_{23}) \geq 1$; such values are observed in star-forming regions, but they are not common (e.g., Pilyugin & Thuan 2005). In this regime, it is unclear which R_{23} branch is appropriate and the diagnostics are not well-calibrated. Furthermore, a very high R_{23} may be an indication of contributions to the line emission from processes not related to star formation. There are nine LIRGs and nine ULIRGs with $R_{23} \geq 1$.

We also assume the upper branch for R_{23} -based diagnostics (Edmunds & Pagel 1984). We use the $[\text{N II}]/[\text{O II}]$ flux ratio as a branch indicator, where all galaxies with $f([\text{N II}])/f([\text{O II}]) > -1$ are assumed to lie on the upper branch (e.g., Kuzio de Naray et al. 2004; see also the theoretical plots of $[\text{N II}]/[\text{O II}]$ and R_{23} vs. abundance in Kewley & Dopita 2002). Eight galaxies (five LIRGs and three ULIRGs) fail this test. Seven of these also surpass the R_{23} threshold; we exclude the remaining LIRG from our analysis, to avoid the problem of stitching together upper and lower branch calibrations (which exists when two different diagnostics are put together; e.g., Salzer et al. 2005). The number of galaxies with low values of $[\text{N II}]/[\text{O II}]$ is interesting, and may

suggest an even larger downward spread in abundance than is found by taking into account only the upper branch systems.

These two cuts do not strongly impact our analysis. Once we put aside galaxies with $z > 0.27$, we have a working sample of 55 LIRGs and 22 ULIRGs. (We discuss further the $z \sim 0.4 - 0.5$ points in §4.4.)

Different diagnostic/calibration pairs can yield very different abundances for the same galaxy. Figure 2 shows the abundance of a random sampling of our galaxies using each method listed above. The methods are ordered on the horizontal axis by increasing median abundance. Over the full sample, the extreme median values (the CL01 Case A and Pilyugin & Thuan (2005) calibrations) differ by a factor of 8 for the LIRGs, and correspond to $12 + \log(\text{O/H}) = 8.2$ and 9.1, respectively. The ‘median of the medians’ is $1.25Z_{\odot}$. For the ULIRGs, the extreme values are 8.1 and 9.0, also a spread of a factor of 8, with the median being roughly $1.0Z_{\odot}$. However, if the Pilyugin & Thuan (2005) diagnostic (the only one in our sample based solely on T_e abundances) is removed, the scatter is dramatically reduced. The peak-to-peak variation among the five remaining diagnostics is only a factor of 2. The median abundances among these five are $1.6Z_{\odot}$ and $1.4Z_{\odot}$ for the LIRGs and ULIRGs, respectively.

In the next subsections we discuss sources of uncertainty.

3.2. Uncertainties in Abundance Caused by Choice of Diagnostic

The lowest abundances arise from the use of the empirically-calibrated diagnostics. This exemplifies the

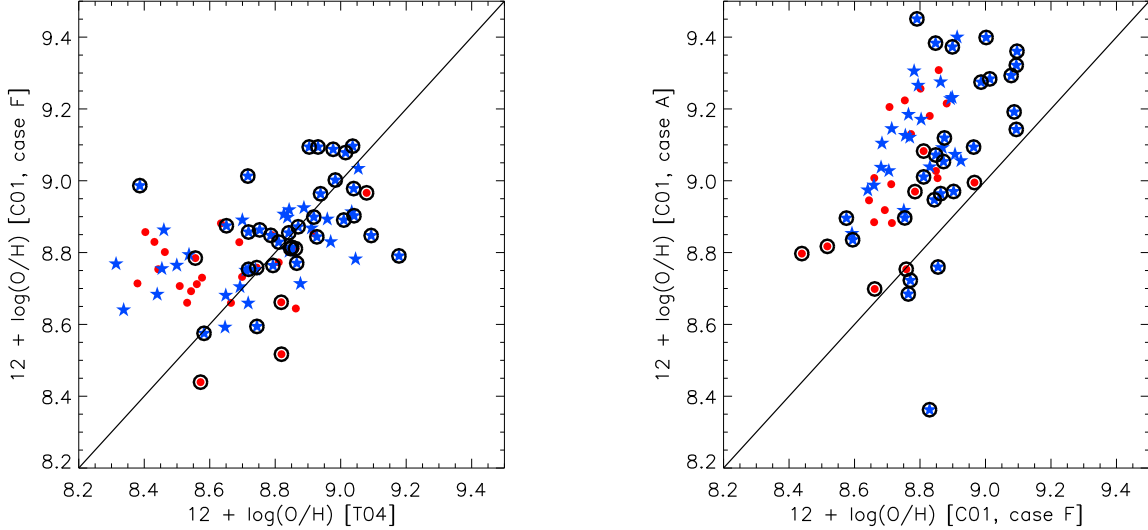


FIG. 3.— Abundance as a function of calibration for (left) Charlot & Longhetti (2001) Case F vs. Tremonti et al. (2004) R_{23} abundances and (right) Charlot & Longhetti (2001) Case A vs. Case F abundances. The former indicates good correspondence on average except at high R_{23} (low Tremonti et al. 2004 abundances). The latter illustrates good correlation but a significant offset between the two, independent of whether or not the galaxies fall inside the SDSS star-forming galaxy locus (Kauffmann et al. 2003). Galaxies inside the locus are circled. Galaxy designations follow Figure 1.

difference between T_e abundances and those from theoretical calibrations. Discussions of the weaknesses of each method are found in Kennicutt et al. (2003) and elsewhere, and we do not expand upon them further. However, we do note that very recent measurements of temperature fluctuations in H II regions coupled with heavy element recombination line measurements may alleviate this discrepancy by raising the T_e abundances (Bresolin 2007). The use of the T_e -calibrated Pilyugin & Thuan (2005) method is thus potentially suspect without an adjustment to agree with these findings. Use of their diagnostic calibration is also a particular challenge for LIRGs and ULIRGs. We compute low values of their ionization parameter variable P ($\langle P \rangle = 0.2$) and relatively high values of R_{23} ($\langle \log(R_{23}) \rangle = 0.7$ for the LIRGs and 0.9 for the ULIRGs). These P/R_{23} combinations are not well calibrated for either branch of the R_{23} vs. abundance diagram in the Pilyugin & Thuan (2005) diagnostic.

Of the photoionization models, those of Kewley & Dopita (2002) produce the lowest dispersion in our sample, as well as the second-highest abundance. The low dispersion is due to the fact that the [N II]/[O II] flux ratio is insensitive to the ionization parameter. One potential problem with this diagnostic calibration is the form assumed for the dependence of the N/O abundance ratio on oxygen abundance. Kewley & Dopita (2002) assume that N/O is constant below $0.23Z_\odot$, and linear in abundance above this value (van Zee et al. 1998). However, the data from recent studies seem to show that N/O may be driven by a linear combination of primary and secondary yields, suggesting a sum of the two contributions rather than an abrupt transition between them. This leads to a slightly higher value of N/O for a given abundance (Bresolin et al. 2005, and references therein). This should lead to a higher value of the flux ratio [N II]/[O II] for a given abundance, and thus a lower derived abundance from the calibration.

Perhaps the most important calibration issue for the results of this paper is the disagreement between the CL01 Case A–F analytic diagnostics and the T04 empirical calibration of R_{23} based on the CL01 models. Rather than comparing all six CL01 diagnostics to T04, we use Cases A and F as representative of the greatest and least amounts of spectral information required by the CL01 models. Figures 2 and 3 illustrate that, while CL01 Case F and T04 agree reasonably well on average, CL01 Case A is higher on average than both by ~ 0.3 dex.

What is the cause of this discrepancy? Either the LIRGs and ULIRGs have line ratios that are affected by processes unrelated to star formation (see the next subsection), or the CL01 Case A diagnostic does not properly account for these objects. Looking at Figures 1 and 3, it is tempting to conclude that Case A, which like the Kewley & Dopita (2002) diagnostic is based on a line ratio involving [N II], predicts higher abundances due to [N II] enhancement by a buried AGN or shocks. Consider the following scenario: AGN and shocks are important for some galaxies, for which the different CL01 diagnostics yield inconsistent abundances; for purely star-forming galaxies, Cases A and F instead give the same result. More specifically, the objects which fall within the SDSS locus of most star-forming galaxies (a criterion which securely excludes galaxies with even a small amount of AGN or shock contribution) should give consistent results for diagnostics A and F of the CL01 model, while those outside this locus should not. Figure 3 reveals that this is not the case: LIRGs and ULIRGs which fall beneath the outer SDSS boundary in the [N II]/H α vs. [O III]/H β line ratio diagram (see Figure 1) show almost as large a disagreement between the CL01 Cases A and F as do the galaxies that lie outside it. Thus, physical effects may have a small contribution, but it appears that most of the difference is attributable to the inability of the Case A diagnostic to properly account for the abundances of these systems. The details of why this

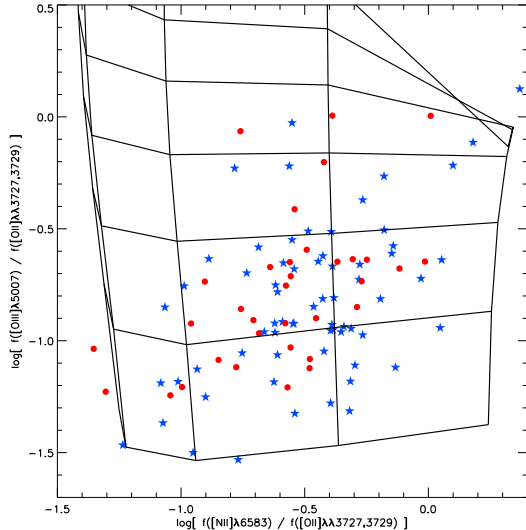


FIG. 4.— $[\text{N II}]\lambda 6583 / [\text{O II}]\lambda 3727, 3729$ vs. $[\text{O III}]\lambda 5007 / [\text{O II}]$, as measured and predicted by theory. These line ratios nicely separate the effects of abundance and ionization parameter, and show that starburst models can in principle explain LIRG and ULIRG line ratios. Abundance increases to the right, with grid points of 0.1, 0.4, 0.8, 2.0, and 4.0 in units of Z_{\odot} . Ionization parameter increases upward, with grid points of (in the log) roughly 1.2 to 3.0, increasing in steps of 0.3 dex. The photoionization models are from Kewley et al. (2001) and use the Starburst99 stellar synthesis code Leitherer et al. (1999) with ‘Lejeune + Schmutz’ stellar atmospheres as an input. These models assume an electron density of 350 cm^{-3} and a continuous starburst of age 8 Myr. Galaxy designations follow Figure 1.

may be so are beyond the scope of this paper. As we discuss in the next subsection, other models are consistent with all of our LIRGs and ULIRGs being star-forming galaxies.

Among the CL01 models, the Case F diagnostic minimizes systematic offsets of LIRGs and ULIRGs with respect to the more sophisticated method by which T04 compute abundances (their method is to find the model spectrum that is the best fit to the entire observed spectrum, rather than using just one or two emission-line ratios). However, as we see in detail in Figure 3, the agreement breaks down at the highest values of R_{23} ; in this regime, the Case F diagnostic gives higher abundances by ~ 0.3 dex. As Figure 2 illustrates, this has little effect on the median abundance. Our use of T04 instead of Case F from CL01 thus makes little difference to the results of this paper. Despite the fact that it is a single-parameter diagnostic, we choose the T04 diagnostic over the Case F diagnostic because it employs the traditional R_{23} line ratio and is the empirical product of a methodologically sophisticated application of the CL01 models.

3.3. Uncertainties in Abundance Caused by Physical Effects

An obvious important consideration is the dust extinction corrections required to derive intrinsic fluxes. (The optical attenuation derived from the Balmer decrement and a foreground screen is $E(B-V) = 0.9$ on average, corresponding to a factor of 3 upward correction to R_{23} to reach the unattenuated line ratio.) LIRGs and ULIRGs have copious quantities of dust in their nuclei;

the emission from this dust creates their high infrared luminosities. The optical line emission we observe does not emerge from the heavily obscured nuclear star clusters in these systems, where almost all of the star formation is occurring (Surace et al. 2000). Presumably it arises instead from star formation occurring near the surface of the nuclear dust cloud, mildly obscured sight lines, or light scattered into the line of sight.

Our use of the Balmer decrement and assumption of an effective foreground screen geometry mean that even our ‘corrected’ line fluxes for these dusty systems will not correspond to their full line luminosities or star formation rates. However, several considerations argue that the *ratios* of our corrected line fluxes will still yield fair estimates of abundances. First, ULIRGs in particular show such large turbulent velocities within their compact nuclear gas structures (e.g., Downes & Solomon 1998) that any abundance gradients should be flattened rapidly once gas has been dumped into a merger’s center of mass. This means that the outer and inner regions of a merger’s dusty core should have similar abundance values. Second, our use of an effective screen geometry is consistent with both (a) the derivation of the Calzetti et al. (2000) attenuation law we have adopted, and (b) in many objects, the measurement of Balmer decrements much higher than could be achieved if H II regions and dust were uniformly mixed (e.g., Thronson et al. 1990). Moreover, tests show that neither use of a Galactic extinction curve (Miller & Mathews 1972) nor assumption of a uniformly mixed geometry (when sources’ observed Balmer decrements allow this) lead to significantly different results. Finally, we emphasize that any relative underestimate of extinction at $[\text{O II}]\lambda 3727, 3729$ would require that the true R_{23} be higher, and therefore the true oxygen abundance lower, than we have reported here. As §§ 4 and 5 make clear, such an adjustment would only strengthen this paper’s conclusions.

A second relevant issue is the applicability of star-formation calibrated abundance diagnostics. As we discuss in §2, LIRGs and ULIRGs deviate from the main body of star-forming galaxies in many line-ratio diagrams (Figure 1). However, they generally lie completely below the Kewley et al. (2001) maximal starburst lines in at least two of these diagrams, and so many or all can plausibly be treated as starbursts.

We illustrate this in Figure 4 by plotting the $[\text{O III}]\lambda 5007 / [\text{O II}]$ line ratio (note this is $0.75 \times \text{O}_{32}$) as a function of $[\text{N II}] / [\text{O II}]$ for each galaxy. Photoionization models from Kewley et al. (2001) are plotted atop the data, assuming a continuous starburst of age 8 Myr. These line ratios nicely separate the effects of abundance and ionization parameter. LIRGs and ULIRGs in this diagram have relatively high abundances and low ionization parameter, though the details depend somewhat on the adopted starburst model.

It remains possible that some objects in our sample may have emission line fluxes with a non-zero contribution from gas that has been photoionized by an AGN or collisionally ionized by shocks. The addition of either a low-luminosity or high-luminosity AGN moves galaxies away from the starburst locus (e.g., Veilleux & Osterbrock 1987; Kewley et al. 2006b). However, it appears that AGN do not make a significant contribution, because mid-infrared diagnostics of ULIRGs

that distinguish starbursts and AGN agree with optical diagnostics if all non-Seyfert ULIRGs are assumed to be starburst-powered (Lutz et al. 1999). The addition of shocks also moves line ratios away from the region of pure starburst galaxies (Dopita & Sutherland 1995). The existence of shocks would be consistent with the presence of massive, fast, galaxy-scale winds in starburst-dominated LIRGs and ULIRGs (Heckman et al. 2000; Rupke et al. 2002, 2005b,c; Martin 2005, 2006). Rupke et al. (2005c) also find evidence that ULIRGs with LINER spectra have higher wind velocities than those with H II spectral types, suggesting that wind shocks could play a role in exciting the observed optical emission lines in LINERs.

Without careful modeling, we cannot easily flag galaxies with significant contributions from low-level AGN or shocks. Rather than attempt an extensive comparison to models of stellar and AGN photoionization or shocks, we make three empirically and theoretically motivated cuts in our data, resulting in three partially overlapping subsamples. Computing our results for each subsample allows us to ascertain the effect of including galaxies with possible low-level AGN or shock contamination. These cuts are as follows: (1) accepting only galaxies which lie beneath the maximal starburst line (Kewley et al. 2001) in the $[\text{O III}]/\text{H}\beta$ vs. $[\text{N II}]/\text{H}\alpha$ and $[\text{O III}]/\text{H}\beta$ vs. $([\text{S II}]\lambda\lambda 6717, 6731)/\text{H}\alpha$ diagrams; (2) accepting only galaxies which lie beneath the maximal starburst line (Kewley et al. 2001) in the $[\text{O III}]/\text{H}\beta$ vs. $[\text{O I}]\lambda 6300/\text{H}\alpha$ diagram; and (3) accepting only galaxies which lie beneath the line denoting the boundary of the locus of SDSS star-forming galaxies (Kauffmann et al. 2003). As shown in later sections, we find that our results are not significantly altered by picking one subsample over another.

A final uncertainty relates to the apertures covered by the spectroscopic observations. Disk galaxies have radial abundance gradients, in the sense that abundance decreases with increasing radius (e.g., Zaritsky et al. 1994). Large apertures covering a significant fraction of the galaxy's light thus lead to lower computed abundances than those covering only the galaxy's inner regions. For the Nearby Field Galaxy Sample (NFGS), covering a range of Hubble types, the average difference between nuclear and integrated abundances is ~ 0.2 dex for nuclear apertures of 1.5 kpc or less (Kewley et al. 2005).

Our spectra include data with a variety of physical apertures, since they are produced with a variety of slit widths and extraction apertures. Our LIRG and ULIRG samples have median redshifts of 0.04 and 0.14, respectively. The LIRG data in particular include one-dimensional spectroscopic apertures $\sim 1'' - 3''$ in width, which corresponds to physical scales of $\sim 1 - 2$ kpc. These qualify more or less as nuclear spectra according to the Kewley et al. (2005) convention for the NFGS. The ULIRG apertures also range from $\sim 1'' - 3''$ in diameter, with about half having small apertures. However, being at higher redshift, they subtend apertures ranging from 2 – 7 kpc. Based on comparison to local field galaxies, we would then expect a slight systemic deviation of the average ULIRG to lower abundances relative to the average LIRG (by ~ 0.1 dex; Kewley et al. 2005). However, the existence of radial abundance gradients in evolved mergers may be inconsistent with expectations of strong radial mixing of heavy elements (L. Kewley 2007,

private communication; Edmunds & Greenhow 1995). If there has been strong radial mixing, aperture size will have little affect on the integrated abundance.

In this work we use two local comparison samples, as well as high redshift data. We defer discussions of aperture effects related to these samples to their points of introduction later in the paper.

With these caveats in mind, we proceed in the next sections to employ the internal consistency of a given abundance diagnostic/calibration pair (the T04 R_{23} calibration in our case) to compare LIRGs and ULIRGs to other galaxy populations.

4. NEAR-INFRARED LUMINOSITY-METALLICITY RELATION

The best way to interpret the abundances of local LIRGs and ULIRGs in the context of galaxy evolution is to compare to the luminosity-metallicity ($L - Z$) and mass-metallicity ($M - Z$) relationships of other star-forming galaxies (i.e., galaxies of lower star formation rate or those selected at other wavelengths). These describe the increase of abundance with increasing galaxy luminosity and mass. They reflect, for a given gas mass fraction, either (a) a sequence of changing star formation history and enrichment with stellar mass or (b) preferential accretion of under-enriched gas or loss of over-enriched gas in low-mass galaxies. Recent authors have argued for both scenarios (T04; Brooks et al. 2007; but see also Köppen et al. 2007 for discussion of an origin in a variable initial mass function). We start with the $L - Z$ relation, since luminosity is a more easily measured quantity than mass.

We compare to the only available near-infrared $L - Z$ relation for starbursts (Salzer et al. 2005). The advantage of using observations in the near-infrared is their lower sensitivity to dust and mass-to-light ratio variations than optical observations (Bell & de Jong 2000; Salzer et al. 2005). The galaxies comprising this study are a subsample of the KPNO International Spectroscopic Survey (KISS; Salzer et al. 2000), which is an objective prism survey of emission-line galaxies in the local universe. The KISS subsample from Salzer et al. (2005) consists of galaxies with near-infrared photometry, mostly taken from 2MASS. The galaxies have $\langle z \rangle = 0.063$ and K_s -band absolute magnitudes ranging from -16.5 up to -25 (a factor of 3000 in luminosity).

Because of the low redshifts and small spectroscopic apertures ($1.5'' - 2''$, corresponding to 2 kpc) for this sample, the computed abundances are approximately nuclear, and we make no aperture corrections.

4.1. NIR photometry

Near-infrared photometry for our LIRG and ULIRG sample is taken from ground-based data in the K' band where available (Surace et al. 2000; Stanford et al. 2000; Kim et al. 2002), and from the 2MASS Large Galaxy Atlas (Jarrett et al. 2003) or Extended Source Catalog (Cutri et al. 2006) otherwise. We use 'total,' or extrapolated, K_s magnitudes from the 2MASS catalog. For some objects with multiple nuclei, a 2MASS magnitude is not available for the nucleus of interest but the sky- and star-subtracted image is available (Cutri et al. 2006). In these cases, we used the 2MASS Atlas images (in 'postage-stamp' form) to do aperture photometry on the nucleus,

including associated diffuse emission. In other instances a second nucleus was already removed through star subtraction, which was to our advantage. However, in the few instances where this subtraction was poor we did the photometric separation by hand. For the ULIRGs with published nuclear and total magnitudes (Kim et al. 2002), we used the relative nuclear magnitudes to scale the total magnitude for the nucleus of interest. Finally, we note that the published FIRST-FSC magnitudes are on average only 70% of the observed total, as discussed in Stanford et al. (2000); in these cases we made an average upward correction to reach $\sim 100\%$.

We converted measured K' magnitudes to K_s magnitudes using the formula from Wainscoat & Cowie (1992); the average $H - K'$ color for H II ULIRGs from Surace et al. (2000) ($\langle H - K' \rangle \sim 0.5$, which applies roughly to LIRGs as well; see Scoville et al. 2000); and the color transformation from CIT system K magnitudes to K_s magnitudes (Cutri et al. 2006).

Starting with the total absolute magnitudes, we contemplated a number of adjustments to the measured luminosities to reach the rest-frame host galaxy luminosity. We decided to apply only one of these adjustments. This involves removal of the central point source in ULIRGs, which is most likely an extremely luminous star cluster (but may also contain part of the central bulge; Surace et al. 2000). Very accurate point-source subtraction is allowed by high-resolution *Hubble Space Telescope (HST)* near-infrared data of ULIRGs (Veilleux et al. 2006). The data for five H II galaxies from this sample have an average point-spread function (PSF) to host-galaxy (PSF-subtracted) luminosity ratio of 0.07, with a range of 0.01 to 0.13. Applying this average correction to each ULIRG lowers its luminosity by an insignificant 0.08 magnitudes.

We also contemplated corrections for dust extinction/emission. Most of the near-infrared light in LIRGs and ULIRGs that are dominated by star formation arises in modestly extinguished stars, not hot dust. For cold, star-forming LIRGs and ULIRGs, most of the near-infrared emission is extra-nuclear (Carico et al. 1990; Scoville et al. 2000; Veilleux et al. 2006), and the colors of this extended light are consistent with those of normal spirals in the case of LIRGs and a reddened stellar population in the case of ULIRGs (Carico et al. 1990; Scoville et al. 2000; Davies et al. 2002). The average predicted screen extinction is modest even for the more heavily extinguished nuclear regions (A_V of a few; Scoville et al. 2000; Surace et al. 2000; Davies et al. 2002). To achieve an unreddened luminosity we would correct upward by only a few tenths of a magnitude (Draine 2003), and even less for the more dominant extended emission. Modest hot dust emission may also contribute to the nuclear light (Surace et al. 2000; Davies et al. 2002), but neither the dust emission nor nuclear light is significant. As a final piece of evidence, ULIRGs tend to show elliptical-like global surface-brightness profiles in the near-infrared, typical of relaxed stellar populations (Veilleux et al. 2002, and references therein).

Finally, we considered K-corrections. There is a strong diversity in observed spectral energy distribution (SED) shapes in ULIRGs, but the average ULIRG shows increasing νL_ν from optical to infrared wave-

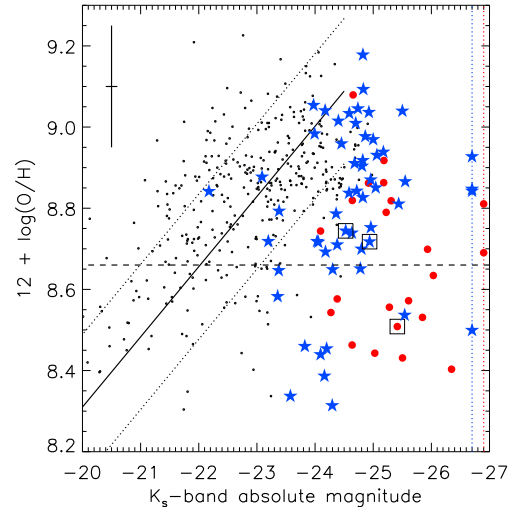


FIG. 5.— K_s band luminosity-metalllicity relation for nearby emission-line galaxies (small black open circles), LIRGs (blue stars), and ULIRGs (red filled circles). Most of the LIRGs and ULIRGs fall well below the $L - Z$ relation. The nearby galaxies are from the KISS sample, and the black line and dotted lines are a fit to the data and 1σ RMS dispersion, respectively (Salzer et al. 2005). The dashed line locates solar abundance. Boxed points do not pass our first emission-line cut. We do not plot points with $z > 0.3$. The far-right points do not have measured K magnitudes.

lengths, and flat or increasing values in the near-infrared (Trentham et al. 1999; Farrah et al. 2003). These yield positive K-corrections in the K -band that increase slowly with increasing redshift and depend somewhat on the actual SED shape (0.06 – 0.25 mag at $z \sim 0.3$ and 0.1 – 0.4 mag at $z \sim 0.6$; Trentham et al. 1999). Given the similarity of the near-infrared colors of LIRGs and ULIRGs (see previous paragraph and references therein), K-corrections for LIRGs are of similar magnitude.

We conclude that the K-corrections, extinction corrections, and corrections for hot dust emission are on average small (a few tenths of a magnitude or less in each case). Given the inherent variations in SEDs and our inability to determine precise adjustments for each galaxy, we choose to ignore these corrections. Regardless, their effect on the following results is negligible. If anything, they are likely to increase the significance of the observed effects.

4.2. $L - Z$ relation

We use the T04 R_{23} abundance calibration to compute upper branch abundances for our LIRGs and ULIRGs for comparison to the KISS results. The resulting K_s -band $L - Z$ relation is shown in Figures 5 – 7. Each figure represents the $L - Z$ relation using a different emission-line cut, as described in §3.3. It is immediately clear that many LIRGs and ULIRGs do *not* fall on this relation, even if we discard possibly shock-excited or AGN-contaminated sources. There is some overlap, however. We also see that the scatter in the computed LIRG and ULIRG abundances for a given magnitude is higher than in the KISS comparison sample.

The observed offset is one of abundance and/or luminosity. If the LIRGs and ULIRGs are over-luminous in the near-infrared with respect to galaxies of lower star formation rates, then there must be a significant (factor

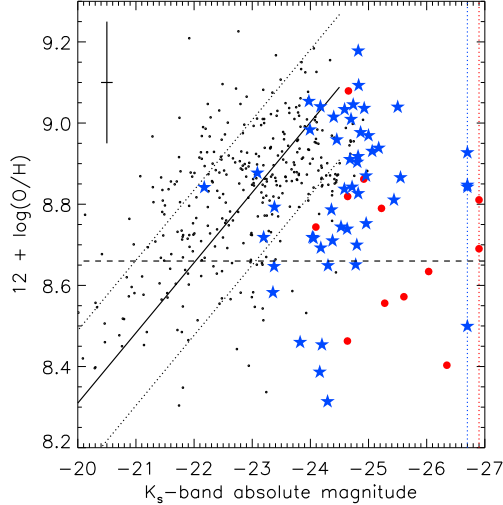


FIG. 6.— $L - Z$ relation, but only for LIRGs and ULIRGs that pass our second emission-line cut. See Figure 5 for more details.

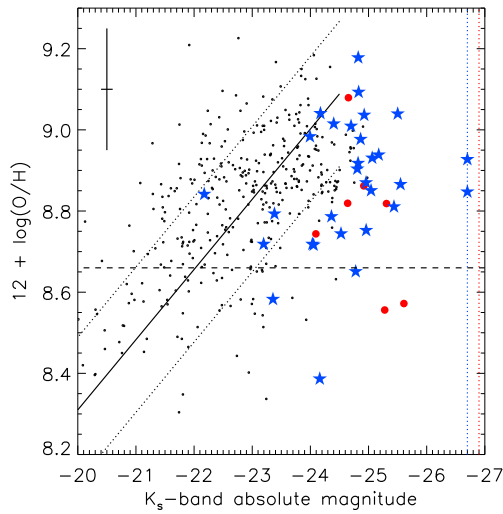


FIG. 7.— $L - Z$ relation, but only for LIRGs and ULIRGs that pass our third emission-line cut. See Figure 5 for more details.

of ~ 10) increase in the near-infrared emission above that from the old, mass-tracing stellar population. As we discuss in §4.1, hot dust could increase the luminosity above that expected from the stellar population, but only by a small fraction of the total. Massive red supergiants from very young star forming regions can also add to the luminosity from old stars while keeping the near-infrared colors almost constant (Leitherer et al. 1999). However, the heaviest young star formation is nuclear, and contributes only a small percentage of the total near-infrared light (§4.1).

We conclude that hot dust and young stars cannot come close to producing a factor of 10 increase in luminosity. Thus, LIRGs and ULIRGs are under-abundant with respect to local, emission-line-selected star-forming galaxies of lower star formation rate. This conclusion is solidified by comparing LIRGs and ULIRGs to the local mass-metallicity relation in §5.

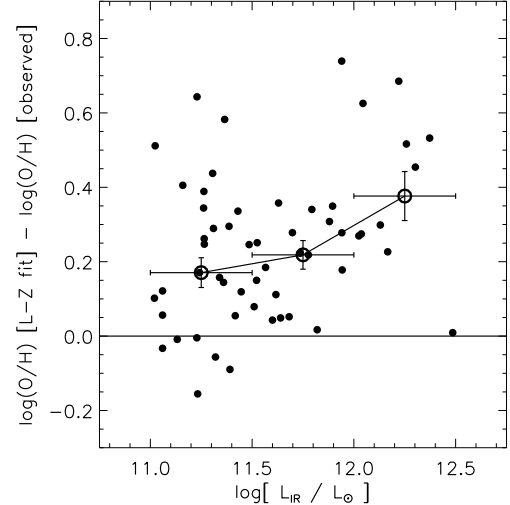


FIG. 8.— Difference between the observed abundances in LIRGs and ULIRGs and the $L - Z$ relation as a function of infrared luminosity. The small filled circles represent individual deviations from the $L - Z$ relation (from the second emission-line cut). The thick open circles are median deviations from $L - Z$ for equal-size bins centered on $\log(L_{\text{IR}}/L_{\odot}) = 11.25, 11.75$, and 12.25 and the error bars represent the standard error in the mean in each bin. LIRGs are offset by 0.2 dex, and ULIRGs by 0.4 dex. Comparison to the $L - Z$ relation shows a mildly significant trend toward higher abundance offsets for higher L_{IR} .

The average galaxy in our sample is more NIR-luminous than the range of luminosities probed by the KISS data (which are biased toward low-luminosity objects because of the required emission-line contrast; Salzer et al. 2005). Thus, there is uncertainty in the shape of the $M - Z$ relation at the luminosities probed by our sample. However, even if the relation is conservatively assumed to flatten above $M_{K_s} \sim -24.5$ rather than to continue to increase, almost all of the observed galaxies are under-abundant compared to the mean oxygen abundance of local, emission-line, modestly star-forming galaxies.

Figure 8 illustrates the offset in abundance from the emission-line galaxy relation as a function of total infrared luminosity L_{IR} for the galaxies passing the second emission-line cut, and conservatively assuming a flat relation above $M_{K_s} \sim -24.5$. Plotting the data in three bins of equal width in $\log(L_{\text{IR}})$ shows qualitatively that galaxies of higher L_{IR} have higher offsets from $L - Z$, with the LIRGs offset by 0.2 dex and the ULIRGs by 0.4 dex. Quantitatively, there is a weak and marginally significant correlation between the two, with the offset increasing by ~ 0.2 dex for each 1 dex increase in L_{IR} . The correlation coefficient is 0.3 regardless of the emission-line cut chosen, while the (parametric) significance of the correlation is 99.7%, 98%, and $\sim 90\%$ for the first, second, and third cuts, respectively, decreasing largely due to the decreasing number of points in each cut. The significance of the correlation depends also on the NIR luminosity at which the flattening is assumed to occur: it increases (decreases) as the cutoff NIR luminosity increases (decreases). It also depends on the emission-line calibration chosen; some calibrations give smaller LIRG-to-ULIRG discrepancies (Figure 2). Finally, we caution that the trends may be weaker than suspected from the

$L - Z$ relation alone (see §5).

4.3. Comparison To Other Merging Systems

LIRG and ULIRG under-abundances are consistent with a recent study of optically-selected mergers (Kewley et al. 2006a). These authors compute the nuclear abundances of a sample of nearby interacting field galaxies with projected separations of $4 - 60$ kpc and optical luminosities $-22 \leq M_R \leq -19$. They find an under-abundance in mergers with respect to the optical B -band $L - Z$ relation for isolated field galaxies. There is a dependence of the offset on separation and ‘central burst strength,’ in the sense that galaxy pairs with small separations ($4 - 20$ kpc) and strong starbursts also have the lowest abundances on average compared to isolated galaxies. They also find that more optically-luminous galaxies have a smaller offset in abundance; for separations of $4 - 20$ kpc and $M_B \gtrsim -21$, the abundance offset is $\lesssim 0.1$ dex.

Local LIRGs and ULIRGs have mean optical luminosities comparable to the highest-luminosity galaxies in the Kewley et al. (2006a) sample, with $M_R \sim -22$ (Veilleux et al. 2002; Ishida 2004). Based on their nuclear separations (Ishida 2004), the non-isolated LIRGs may represent similar galaxy interaction states compared to the optically-selected galaxies. The mean ratio of present-to-past star formation is higher in LIRGs, however, based on the higher $H\alpha$ equivalent widths in LIRGs (Veilleux et al. 1995; Barton et al. 2000). The ULIRGs represent stronger or more highly progressed galaxy interactions with much higher star formation rates compared to the optically-selected mergers. This conclusion is based on the structural properties of ULIRGs (Veilleux et al. 2002) and their high $H\alpha$ equivalent widths (Veilleux et al. 1999). More indirectly, ULIRGs are scarce in the local universe relative to the parent sample of the optically-selected pairs (Falco et al. 1999).

The observed differences between LIRGs and ULIRGs and isolated galaxies of lower star formation rate reflect a continuation of the trends observed by Kewley et al. (2006a). LIRGs and ULIRGs are more strongly offset from the K -band $L - Z$ relation (by $0.2 - 0.4$ dex) than are galaxies of similar R -band luminosity from the B -band $L - Z$ relation ($\lesssim 0.1$ dex; Kewley et al. 2006a). As we describe above, they also are stronger or later stage interactions and/or have stronger starbursts.

Within our sample, the apparent trend of greater abundance offset with increasing infrared luminosity (Figure 8) mirrors the correlation of abundance offset with starburst strength found in optically-selected mergers. We also studied the dependence of offset on projected nuclear separation. No significant relationship was found, unlike the optical sample. This most likely reflects either (a) the saturation of the sensitivity of nuclear separation to interaction timescale or merger age as two nuclei merge and/or (b) a greater correlation of $L - Z$ offset with level of star formation than with nuclear interaction state.

4.4. Comparison To High Redshift

Comparison of luminosity-metalllicity and mass-metalllicity relations at low and high redshift point to chemical evolution of galaxies over cosmic time (Lilly et al. 2003; Kobulnicky & Kewley 2004; Maier et al. 2005; Savaglio et al. 2005; Erb et al. 2006;

Mouhcine et al. 2006). As mentioned in §1, high-redshift abundance measurements of a modest number of LIRGs selected at $15 \mu\text{m}$ and ULIRGs selected at submillimeter wavelengths exist (Liang et al. 2004; Swinbank et al. 2004; Tecza et al. 2004; Nesvadba et al. 2007). Three of these studies are based on R_{23} abundances, while the third (Swinbank et al. 2004) relies on the $[\text{N II}]/\text{H}\alpha$ flux ratio, a slightly less robust indicator. From our work, we also have data on four LIRGs and ULIRGs at $z \sim 0.4 - 0.5$ (Rupke et al. 2005b). Because near-infrared photometry for many of these sources exist (Liang et al. 2006; Hammer et al. 1997; Smail et al. 2004), we can compare them directly to our data on the K -band $L - Z$ relation.

Of the $15 \mu\text{m}$ sources from Liang et al. (2004), we select only those which have infrared luminosities consistent with the definition of LIRGs. We assume the K -correction is small and do not apply it. However, we do adjust the magnitudes listed in Liang et al. (2006) downwards by 1.9 magnitudes to convert from the AB to the Vega photometric system, as they are listed as AB magnitudes in Hammer et al. (1997). (The magnitude of Vega in the AB system is taken from Tokunaga & Vacca 2005.) We also apply upward aperture corrections of 0.1 dex to reach nuclear abundances, following the treatment of local disk galaxies in Kewley et al. (2005).

All of the submillimeter galaxies (SMGs) in Swinbank et al. (2004) have ULIRG-like or higher total infrared luminosities. To compare them to the local near-infrared $L - Z$ relation, we apply K-corrections to the K -band observed magnitudes from Smail et al. (2004) using the average $z = 2$ ULIRG-derived correction from Trentham et al. (1999) of 0.45. We also discard galaxies with very broad $H\alpha$ ($\text{FWHM} > 1500 \text{ km s}^{-1}$) and/or $\log([\text{N II}]/\text{H}\alpha) > -0.1$. This is an attempt to eliminate galaxies with AGN and/or with emission lines contaminated by shock excitation, respectively.

Because of limited emission-line data, we compute SMG abundances using the ‘coarse’ calibration from Salzer et al. (2005) that employs $[\text{N II}]\lambda 6583/\text{H}\alpha$ (and is derived from the T04 R_{23} relation). The exception is SMM J14011+0252, for which we use the R_{23} diagnostic with the data from Nesvadba et al. (2007). Comparison of the $[\text{N II}]/\text{H}\alpha$ and R_{23} diagnostics for local ULIRGs suggest that at low abundances the former tends to over-predict the abundance by an average factor of ~ 2 . This is unsurprising given the results of the application of other $[\text{N II}]$ -based diagnostics to LIRGs and ULIRGs (§3.2).

In Figure 9, we plot the $L - Z$ data for local LIRGs and ULIRGs, for $z = 0.4 - 0.9$ LIRGs and ULIRGs, and for $z \sim 2$ SMGs. For SMM J14011+0252, we plot the abundances of both nuclei, J1n and J1s. Figure 10 makes this comparison more quantitative. The results show that the LIRGs evolve upward in abundance by ~ 0.2 dex from $z \sim 0.6$ to the present day, as would be expected from continual processing of heavy elements in their progenitors. For the $z \sim 0.5$ ULIRGs, we are limited by number statistics, but there is a suggestion of evolution.

The very high redshift systems, the SMGs at $z \sim 2$, show a large scatter in abundances. This is partly due to low emission-line sensitivity at these redshifts, the coarse diagnostic required to compute the abundance, and the difficulty in weeding out AGN or shock-excited candidates. Furthermore, the SMGs are much more near- and

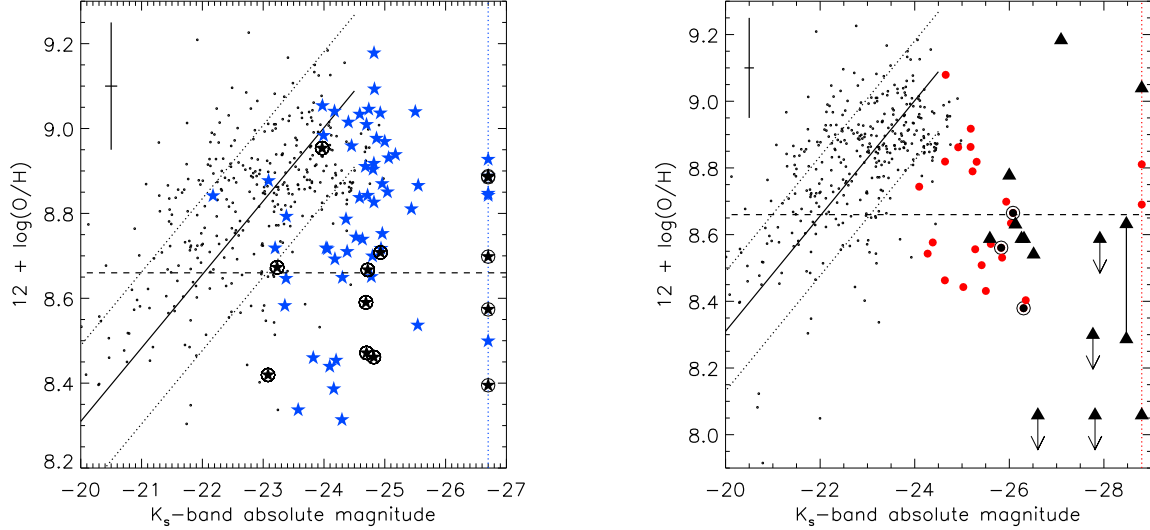


FIG. 9.— Redshift evolution of the LIRG (left) and ULIRG (right) L-Z relations. See Figure 5 for more details. We show here data that pass the first emission-line cut. (a) The black, encircled stars are LIRGs with $0.4 < z < 0.9$ from Liang et al. (2004, 2006), supplemented with one point from this work. (b) The black, encircled circles are ULIRGs with $z \sim 0.4 - 0.5$ from this work. The black triangles are submillimeter-selected galaxies with $1.4 < z < 2.7$ and luminosities equal to or greater than those of ULIRGs (Smail et al. 2004; Swinbank et al. 2004). The vertical line connects the abundances for the two nuclei of SMM J14011+0252 (Nesvadba et al. 2007).

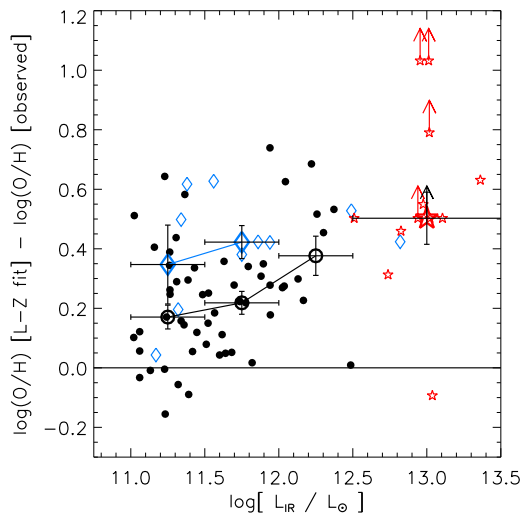


FIG. 10.— The abundance offset from the local $L - Z$ relation for low- and high-redshift LIRGs and ULIRGs, as a function of infrared luminosity. We show here data that pass the second emission-line cut. The (black) small filled circles, (blue) small open diamonds, and (red) small open stars represent $z \sim 0.1$ LIRGs and ULIRGs from this work, $z \sim 0.6$ LIRGs and ULIRGs from Liang et al. (2004) and this work, and $z \sim 2$ SMGs (Swinbank et al. 2004; Nesvadba et al. 2007), respectively. The (black) thick open circles, (blue) thick open diamonds, and (red) thick open star are median deviations from $L - Z$ for local LIRGs and ULIRGs, $0.4 < z < 0.9$ LIRGs, and $z \sim 2$ SMGs, respectively. The LIRGs clearly evolve upward in abundance by ~ 0.2 dex from $z \sim 0.6$ to $z \sim 0.1$, as would be expected from continual processing of heavy elements. Though there only 2 $z \sim 0.5$ ULIRGs in this figure, there is also apparent redshift evolution in ULIRG abundance from $z \sim 0.5$ to $z \sim 0.1$. Finally, there is also evidence for modest evolution from $z \sim 2$ SMGs to $z \sim 0.1$ ULIRGs, though the observed scatter and systematic uncertainties are large.

far-infrared luminous than ULIRGs, so the comparison may not be appropriate. Despite these caveats, there is a suggestion of abundance evolution on average.

5. MASS-METALLICITY RELATION

Galaxy mass is a somewhat more fundamental quantity than instantaneous luminosity (i.e., it is more useful for predicting a galaxy's properties). The mass-metallicity relation is thus a better tool than the luminosity-metallicity relation for quantifying the implications of LIRG and ULIRG abundances for galaxy evolution. However, mass has its own set of limitations; for instance, mass is less easily measured than luminosity. In this section, we compare the masses and abundances of LIRGs and ULIRGs to those of nearby star-forming galaxies from the SDSS (T04).

The stellar masses for the ULIRGs are estimated from dynamical mass measurements. These are based on near-infrared measurements of central stellar velocity dispersions and rotational velocities (Dasyra et al. 2006b). We do not have individual measurements for most (2/3) of the ULIRG nuclei in our sample. To plot individual nuclei on the $M - Z$ relation, we instead use the high-precision average mass and observed scatter of merger remnant nuclei from Dasyra et al. (2006b) to assign masses to the ULIRGs in our sample. The variance in mass is computed from the mass equation and the observed scatter in random and rotational velocities. The mass of each galaxy is then drawn from a Gaussian random distribution of the proper mean and variance, with the limitation that the mass cannot deviate by more than 3σ from the mean.

Direct stellar mass measurements for LIRGs do not exist in the literature. However, the indirect method of modeling galaxy spectra suggests an average stellar mass in star-forming LIRGs that is one-half that of a ULIRG merger remnant ($\sim 5 \times 10^{10} M_{\odot}$; Pasquali et al. 2005). This is consistent with some LIRGs being progenitor ULIRGs (Ishida 2004). A caveat is that the Pasquali et al. (2005) galaxies have $\log(L_{\text{FIR}}/L_{\odot}) = 10.5 - 11.5$, rather than the range $\log(L_{\text{IR}}/L_{\odot}) = 11.0 - 12.0$ normally assigned to LIRGs (note that $L_{\text{FIR}} < L_{\text{IR}}$

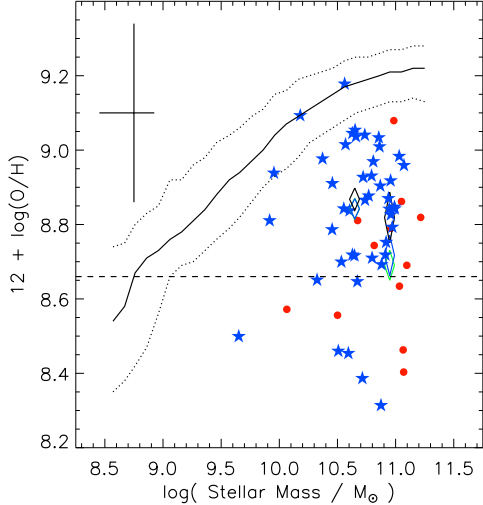


FIG. 11.— Comparison of the mass-metallicity relation from the SDSS (Tremonti et al. 2004) with LIRG and ULIRG abundances and stellar masses. The average LIRG and ULIRG are significantly under-abundant, as they are when compared to the $L - Z$ relation. The dotted lines show 1σ scatter on either side of the mean SDSS relation, which has been shifted upward by 0.1 dex to account for aperture effects. Atop this relation are median LIRG and ULIRG abundances (colored diamonds). The diamond colors represent different emission-line cuts (cut 1, green; cut 2, blue; cut 3, black), and the sizes represent the dispersion in points (the standard error in the median). We also plot individual abundance measurements under the second emission-line cut, randomly distributed in mass according to the measured mean and standard deviation for LIRGs and ULIRGs (Pasquali et al. 2005; Dasyra et al. 2006b).

by $\sim 10\%$; Sanders & Mirabel 1996). Regardless, our comparison to $M - Z$ does not depend sensitively on our choice of LIRG mass. As with the ULIRGs, the mass of each galaxy is drawn from a Gaussian random distribution of the proper mean and variance. We assume that the mean equals one-half the mean for ULIRGs but that the variance in linear mass space is the same.

The SDSS galaxies to which we compare are primarily late-type (T04), so their disks presumably have abundance gradients. The physical diameter spanned by the SDSS spectroscopic fiber is relatively large ($3''$, corresponding to 4.6 kpc at $\langle z \rangle = 0.08$). Using trends of abundance dilution as a function of aperture size gleaned from the NGFS data (Kewley et al. 2005), we correct the SDSS abundances upward by 0.1 dex so that they better approximate nuclear abundances.

The $M - Z$ relation is shown in Figure 11 with the LIRG and ULIRG points over-plotted. The results are comparable to those obtained when we compare LIRGs and ULIRGs to the $L - Z$ relation. LIRGs and ULIRGs are significantly offset from the $M - Z$ relation, regardless of the emission-line cut chosen. We also observe a much larger scatter in the abundances of LIRGs and ULIRGs than in the reference sample at a similar mass.

In the case of $M - Z$, the offsets from the mean relation are unambiguously ones of abundance rather than mass, since the progenitors of LIRGs and ULIRGs are massive spirals. In Figure 12, we plot the abundance offsets of LIRGs and ULIRGs from the $M - Z$ relation as a function of infrared luminosity atop the same offsets computed using the $L - Z$ relation. In each case we use data that pass the second emission-line cut. The median

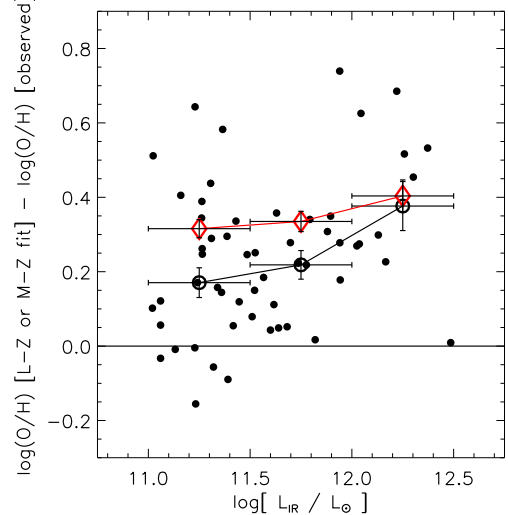


FIG. 12.— Difference between the observed abundances in LIRGs and ULIRGs and the $L - Z$ and $M - Z$ relations, as a function of infrared luminosity. The (red) thick open diamonds are median deviations from the $M - Z$ relation. There is excellent qualitative agreement between the two, though comparison to the $M - Z$ relation yields a slightly larger under-abundance of the LIRGs than does comparison to the $L - Z$ relation. Refer to Figure 8 for more details.

offset of ULIRGs from the $M - Z$ relation, 0.4 dex, is the same as the offset from the $L - Z$ relation (with our conservative flattening assumption), but the offset from the $M - Z$ relation is higher for the LIRGs at 0.3 dex (vs. 0.2 dex from the $L - Z$ relation). The correlation between L_{IR} and under-abundance may be present in the $M - Z$ offsets as it is in the $L - Z$ offsets, but the observed trend is weaker and not significant. Nevertheless, given the systematic uncertainties in abundance diagnostic calibrations, individual luminosity corrections, individual masses, and the exact shape of the $L - Z$ relation, we conclude that the $L - Z$ and $M - Z$ offsets are in good agreement with one another.

6. EFFECTIVE YIELD

Using our measurements of the gas-phase abundances of oxygen in LIRGs and ULIRGs, we are able to compute effective yields. The true yield p is the fraction of the mass of a generation of stars that is converted into a heavy element (in this case, oxygen) and returned to the ISM. More precisely, for a given stellar generation, p refers to the total mass of a heavy element produced by massive, short-lived stars normalized by the mass locked up in long-lived stars and stellar remnants. The related quantity of effective yield is defined as $p_{eff} \equiv Z / \ln(\mu_g^{-1})$, where $\mu_g \equiv M_{gas} / [M_{gas} + M_{stars}]$ is the gas mass fraction and $Z \equiv M_{heavy\ element} / M_{gas}$. The effective yield provides information on the chemical history of the galaxy through comparison with detailed evolutionary models. In the case of a ‘closed-box’ model with instantaneous recycling, the effective yield equals the true yield ($p = p_{eff}$).

The effective yield is more sensitive to the chemical history of galaxies than the $M - Z$ relation alone, since it also incorporates information about the present gas content of the galaxy. Star formation increases a galaxy’s effective yield until it asymptotically reaches the true yield,

by consuming gas and producing metals. Conversely, gas flows in and out of the galaxy reduce the effective yield (e.g., Edmunds 1990; Köppen & Edmunds 1999; Dalcanton 2007). An exception is the case of inflows of gas with non-zero abundance. Elementary models of radial inflow in galaxy disks suggest that they can increase the effective yield above the true yield by small amounts (factors of 2 or less; Edmunds & Greenhow 1995).

A typical ULIRG gas mass fraction can be determined from global H I and H₂ observations. Some uncertainty exists due to the fact that the conversion of CO molecular luminosities to H₂ gas masses differs between ULIRGs and normal galaxies and is not known exactly (cf., Sanders et al. 1991; Downes & Solomon 1998). The uncertainty is compounded by the scarcity of H I measurements of ULIRGs. We use the best available data on ULIRG gas masses (Mirabel & Sanders 1988, 1989; Sanders et al. 1991; Downes & Solomon 1998), and the average stellar mass of single nucleus ULIRGs from Dasyra et al. (2006a). We then consider ranges of possible values for the H I mass fraction and CO-to-H₂ conversion factor, arriving at an average gas mass fraction in ULIRGs of $\langle \mu_g \rangle = 0.1 \pm 0.05$. (The conservative uncertainty estimate is dominated by our uncertainty in M_{HI}/M_{H_2} .) This estimate is roughly consistent with the gas mass fraction estimated from gas dynamical measurements ($M_{gas}/M_{dyn} \sim 0.16$; Downes & Solomon 1998). As expected, it is also much lower than the gas mass fractions of high-redshift, submillimeter-selected ULIRGs ($\langle \mu_g \rangle = 0.3 - 0.5$; Greve et al. 2005; Tacconi et al. 2006).

In the case of LIRGs, M_{HI}/M_{H_2} is better constrained by measurements (Mirabel & Sanders 1989; Sanders et al. 1991). The value of M_{H_2}/L'_{CO} is also lower than in normal galaxies, though its value relative to that in ULIRGs is uncertain. An additional uncertainty arises due to the absence of accurate stellar mass measurements in LIRGs. We resort to assuming that the stellar mass of a LIRG is one-half that of a ULIRG (as in §5). Again, using the best measurements available and bracketing different possibilities, we estimate $\langle \mu_g \rangle = 0.2 \pm 0.1$. (In this case, the conservative uncertainty estimate is dominated by our uncertainties in the stellar mass and M_{H_2}/L'_{CO} .)

Figure 13 displays the median effective yields of oxygen in LIRGs and ULIRGs compared to the T04 mass-effective yield relation. LIRGs and ULIRGs have significantly lower effective yields, by factors of 2 and 3.5, respectively. This result mirrors the under-abundances described in previous sections, since (a) p_{eff} is linearly proportional to oxygen mass fraction and (b) the LIRG and ULIRG gas mass fractions (0.2 and 0.1, respectively) are similar to those of the average SDSS emission-line galaxy of similar mass ($\mu_g = 0.2$ for $M \sim 10^{11} M_\odot$). This result is robust even if we have seriously underestimated μ_g in ULIRGs: if μ_g in ULIRGs is raised to 0.2, p_{eff} is still significantly lower (by a factor of 2.5) in ULIRGs than in the SDSS galaxies.

7. DISCUSSION

What is the cause of the $L - Z$ and $M - Z$ under-abundances (Figures 5–7 and 11)? It is accepted that the average progenitors of LIRGs and ULIRGs are gas-rich spirals (Barnes & Hernquist 1996; Mihos & Hernquist 1996; Veilleux et al. 2002; Iono et al. 2004; Ishida 2004;

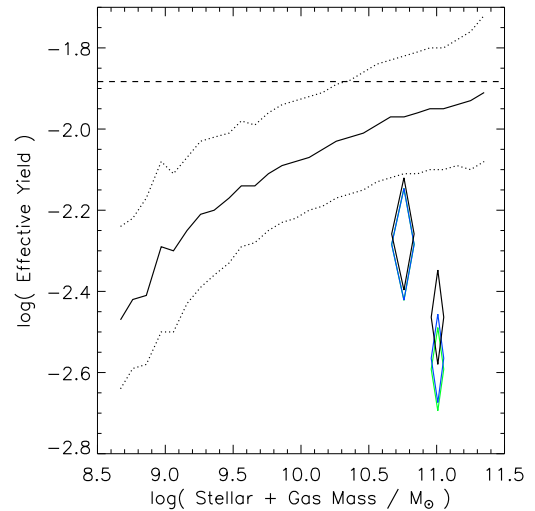


FIG. 13.— LIRG and ULIRG average effective yields compared to the mass-effective yield relation from the SDSS (Tremonti et al. 2004). The average LIRG and ULIRG have effective yields that are lower than the average SDSS galaxy of the same masses by factors of 2 and 3, respectively, as a consequence of abundance dilution. The yields are computed using the median abundances for LIRGs and ULIRGs and gas mass fraction estimates of $\mu_g = 0.1 \pm 0.05$ and 0.2 ± 0.1 , respectively. See Figure 11 for an explanation of most of the lines and symbols. The horizontal dashed line is the SDSS estimate of the true yield. The SDSS yields have been shifted upward by 0.1 dex to account for aperture effects.

Naab et al. 2006). Prior to an interaction and the ensuing intense star formation episode, these progenitor spirals presumably lie on the $L - Z$ and $M - Z$ relations. Since star formation increases the abundance of a system, the only processes that can reduce it are gas motions (Edmunds 1990; Köppen & Edmunds 1999; Dalcanton 2007).

Almost all LIRGs and ULIRGs host fast, massive, and powerful outflows (Heckman et al. 2000; Rupke et al. 2002, 2005a,c; Martin 2005, 2006). The hot phase of these outflows is enriched in oxygen relative to iron (e.g., Grimes et al. 2005). This enrichment arises because the hot phase consists of supernovae ejecta from the current generation of star formation. Expulsion of these metal-rich ejecta therefore cannot in principle reduce the abundance of the galaxy below its value prior to the starburst. Rather, outflow of hot gas prevents further enrichment.

There exists also a neutral, much cooler gas phase in these outflows with mass several times that in the hot phase (Rupke et al. 2005c)³. The average neutral gas mass in LIRG and ULIRG winds is estimated to be $10^9 M_\odot$ (Rupke et al. 2005c), or $\sim 10\%$ of the average total gas mass. The effect on the galaxy's ISM is thus significant, and outflows could remove the bulk of the galaxy's ISM over long timescales (10^8 – 10^9 yr) if they act continuously. The outflowing neutral gas is swept up from the disk of the galaxy and has abundance equal to that of the nuclear star-forming region. Therefore,

³ Rupke et al. (2005c) write that the mean M_{cold}/M_{hot} in LIRGs and ULIRGs is ~ 0.5 . However, the normalization of the model that was compared to the observations is in error. Correcting it implies that the actual entrainment value is ~ 10 in LIRGs and ~ 2 in ULIRGs, with an average of a few and a large scatter (from 0.25 to 20).

despite its large mass, the neutral phase of LIRG and ULIRG outflows cannot reduce the abundance of the nuclear regions, since it is not preferentially removing heavy metals from the ambient gas.

Significant radial inflow of gas also occurs in gas-rich mergers (e.g., Barnes & Hernquist 1996; Mihos & Hernquist 1996; Iono et al. 2004; Naab et al. 2006). Transfer of angular momentum from gas to stars through gravitational torques and dissipation of kinetic energy in shocks causes much of the gas of the progenitor systems to flow inward during the merger. Naab et al. (2006) study the merger of two disk galaxies of equal mass, each with $\mu_g = 0.1$. On the galaxies' first pass (the LIRG phase), 10 – 60% of the gas in each disk flows inward to small radii (with the exact value depending on geometry). During the final coalescence (the ULIRG phase), 50 – 85% of the total gas moves to the nucleus. The final increase in the central gas mass is by a factor 3 – 4 within a 2 kpc radius (Iono et al. 2004).

Radial abundance gradients exist in most disk galaxies, such that abundances of oxygen and other elements decrease with increasing distance from the galactic center (e.g., Zaritsky et al. 1994). Inflow of gas consequently moves gas of low abundance into a nuclear region whose initial abundance is higher. As a result, the central regions of LIRGs and ULIRGs would naturally exhibit lowered abundances due to dilution. The dilution of the nuclear abundance Z is given by $Z_{final}/Z_{initial} = (1 + ab)/(1 + a)$, where a is the ratio of gas mass arriving in the nucleus to that of gas already present and b is the ratio of abundances of the inflowing and nuclear gas. For LIRGs and ULIRGs we have shown that $Z_{final}/Z_{initial} \sim 0.5$, and simulations predict $a = 3 – 4$ (Iono et al. 2004). Inverting the above equation and solving for b , we find $b = 0.35$ (i.e., the inflowing gas had 35% of the initial abundance of the nuclear gas). This is consistent with the mean oxygen abundance gradient observed in spirals (-0.6 dex per isophotal radius, or 25% of the nuclear abundance at the isophotal radius; Zaritsky et al. 1994).

The effective yield of a galaxy can also change under a variety of processes (§ 6). However, in our case the low effective yields we observe are primarily due to low abundances. There is a secondary effect on p_{eff} due to changes in μ_g , but the effect is small for these systems (§6). Thus, the effective yields in LIRGs and ULIRGs have been lowered primarily by the same processes that have lowered the abundances.

The inflow scenario was proposed to explain the offset of local, optically-selected interacting pairs from the B -band $L – Z$ relation (Kewley et al. 2006a). Our arguments above, based on reduced abundance and effective yield, clearly make it the preferred explanation for these infrared-selected mergers, as well. As we discuss in §4.3, the offsets from the $L – Z$ relation in LIRGs and ULIRGs are larger than those in optically-selected mergers. Our interpretation implies that more gas has been funneled to the centers of LIRGs and ULIRGs than in the optical mergers. This parallels the observation that ULIRGs are later-stage mergers and that LIRGs and ULIRGs have higher star formation rates than the optical mergers. The amount of gas channeled to the center increases with merger age (e.g., Naab et al. 2006),

and star formation is powered by the gas driven to the merger center (e.g., Mihos & Hernquist 1996).

The differences between the optical and infrared mergers could also arise from their different chemical evolutionary histories following inflow. We have concluded that under-abundances in the infrared-selected systems must be caused by gas inflow. Following a major inflow event, closed-box consumption of gas by star formation in LIRGs and ULIRGs will tend to elevate the gas-phase abundances of heavy elements, while strong outflows of metal-rich supernovae ejecta will maintain low abundances. Thus, the abundance dilution due to inflow may have initially been stronger than observed, depending on the subsequent effects of star formation and outflow.

The degree to which the initial under-abundance created by inflow was smaller than the observed value can in principle be determined from the properties of the ensuing star formation and outflow. In practice, the degeneracy among quantities such as the amount of gas consumed by star formation, the amount of gas ejected by outflows, and the enrichment of the outflowing gas means that such an exercise is not well-constrained. Simply from the good agreement between the observed under-abundances and those expected from our basic calculations of abundance dilution, we tentatively conclude that the abundance immediately after inflow cannot be much lower than the abundance observed now. In Appendix A, we present example calculations that show subsequent abundance evolution due to star formation and outflows need not undermine this argument. The uncertainties are too large to make quantitatively useful statements about the impact of star formation and outflows. However, these calculations do serve to illustrate that the scatter in abundances we observe may be due to galaxy-to-galaxy differences in how the inflow, star formation, and outflow have proceeded.

8. SUMMARY AND OUTLOOK

We have shown that luminous and ultraluminous infrared galaxies do not follow the standard luminosity-metallicity and mass-metallicity relations for isolated galaxies with lower star formation rates. As a consequence, their effective yields are also smaller than those of similar-mass galaxies.

We conclude that there is an oxygen under-abundance in the nuclei of LIRGs and ULIRGs, compared to galaxies of the same luminosity and mass. We attribute this to radial inflow of gas into the galaxy nuclei, as was concluded for studies of optically-selected mergers (Kewley et al. 2006a). This is consistent with the fact that many LIRGs and all ULIRGs are in the early and late stages, respectively, of a merger of two roughly equal-mass galaxies. Other LIRGs are involved in more minor interactions and/or mergers. These interactions and mergers cause gas from large radii, which is less oxygen-abundant than the central regions, to fall to the center and dilute the nuclear abundance. This infalling gas also fuels star formation; LIRGs and ULIRGs manifest the highest star formation rates in the local universe.

Consistent with this interpretation is the observation that the LIRGs and ULIRGs have larger offsets from the $L – Z$ relation (0.2–0.4 dex) than optically-selected mergers of similar luminosity ($\lesssim 0.1$ dex; Kewley et al. 2006a).

The LIRGs and ULIRGs are in more extreme interaction states and/or have much higher star formation rates than the optically-selected mergers.

A consequence of this result is that the $L - Z$ and $M - Z$ relations are not universal. At $z \gtrsim 0.5$, where the star formation rate density of the universe is dominated by LIRGs and ULIRGs (e.g., Le Floc'h et al. 2005; Caputi et al. 2007), the $L - Z$ and $M - Z$ relations for star-forming galaxies will be governed by mergers (Smail et al. 2004; Shi et al. 2006; Bridge et al. 2007, though see also Melbourne et al. 2005). Observations of high-redshift $L - Z$ and $M - Z$ relations that reveal a relation shifted to lower abundance and/or higher luminosity and mass must account for this. For instance, the optically-selected galaxies at $z \sim 2$ that were used to assess the evolution of $M - Z$ are mostly LIRGs (Erb et al. 2006; Reddy et al. 2006). A large part of the offset attributed to evolution may be due to the fact that the relations include more galaxies that are the by-product of merging. These high- z mergers would have lower abundances not only because they are younger but also because they have undergone gas inflow.

Our low-redshift sample thus represents a baseline for comparison to abundances of high-redshift LIRGs and ULIRGs. The abundances of high-redshift luminous infrared galaxies should be compared only with the abundances of local galaxies with comparable star formation rate and/or interaction strength, not with the abundances of field galaxies of low star formation rate. We compare our sample to a small sample of LIRGs at $0.4 < z < 0.9$ (Liang et al. 2004) and find an increase in abundance with decreasing redshift (~ 0.2 dex from $z \sim 0.6$ to $z = 0.1$). Three $z \sim 0.5$ ULIRGs from the current sample also have lower abundances than the $z = 0.1$ mean. The situation for extremely luminous, high-redshift SMGs (Swinbank et al. 2004; Tecza et al. 2004; Nesvadba et al. 2007) is unclear, however; our upper limit on the mean abundance is consistent with red-

shift evolution but more data are needed. Many more optical and near-infrared spectra of $z > 0.5$ LIRGs and ULIRGs are necessary to understand the abundance evolution of infrared-selected mergers.

The authors are grateful to Stéphane Charlot, Don Garnett, Lisa Kewley, Stacy McGaugh, John Salzer, and Alice Shapley for helpful discussion. John Salzer kindly provided us with the KISS abundance data for use in our figures. Lisa Kewley also graciously provided an IDL script which was the initial framework for computing the abundances presented herein. DSNR and SV were supported by the following AST grants from the NSF: CAREER 9874973, ATI 0242860, and EXC 0606932.

Some of the observations reported here were obtained at the W. M. Keck Observatory, which is operated as a scientific partnership among Caltech, the University of California, and NASA; and the MMT Observatory, which is a joint facility of the Smithsonian Institution and the University of Arizona. The Keck Observatory was made possible by the generous financial support of the W. M. Keck Foundation; we thank those of Hawaiian ancestry on whose sacred mountain the Observatory stands. Our research has made use of IRAF, which is distributed by the National Optical Astronomy Observatories; the NASA/IPAC Extragalactic Database (NED), which is operated by JPL/Caltech under contract with NASA; data products from the Two Micron All Sky Survey, which is a joint project of the University of Massachusetts and IPAC/Caltech and funded by NASA and NSF; and the Sloan Digital Sky Survey, which is funded by the Alfred P. Sloan Foundation, the Participating Institutions, the NSF, the U.S. Department of Energy, NASA, the Japanese Monbukagakusho, the Max Planck Society, and the Higher Education Funding Council for England. The SDSS is managed by the Astrophysical Research Consortium for the Participating Institutions.

APPENDIX

MODELS OF POST-INFLOW ENRICHMENT

To illustrate interstellar chemical evolution in LIRGs and ULIRGs subsequent to gas inflow, we present two example calculations, one using a simple closed-box and the other a modified leaky-box model. In these examples, we assume the true oxygen yield of $p = 0.0131$ from T04, adjusted upward by 0.1 dex according to our aperture corrections. We refer to the oxygen abundance by mass after inflow and before star formation and outflow as Z_1 , and the observed abundance as Z_2 . We use the average observed value of $Z_2 \sim 0.006$ from this paper (in the T04 calibration). Similarly, the galaxy's gas masses before and after star formation/outflow are M_1 and M_2 . For simplicity, we choose a single value of $M_2/M_1 = 0.8$ as a reasonable guess (i.e., 20% of the galaxy's gas has been consumed in star formation and/or ejected by outflows). Exactly how much gas has been consumed by star formation is unclear, but we do know that the gas-consumption timescale in ULIRGs is short ($\lesssim 100$ Myr; Downes & Solomon 1998). Because our goal is simply to illustrate that Z_2/Z_1 can be minimized, we leave it to the reader to try other values of M_2/M_1 .

In the closed-box model (Talbot & Arnett 1971), Z_1 is given by

$$Z_1(\text{closed box}) = Z_2 + p \ln(M_2/M_1). \quad (\text{A1})$$

Substituting the values listed above, we find $Z_1 = 0.003$, or half the present-day value. In the closed-box model with the values listed above, consuming more than half of the gas present ($M_2/M_1 \lesssim 0.5$) implies that $Z_1 < 0$, which is unphysical.

In a leaky-box model (Hartwick 1976), outflows eject from the galaxy some or all of the heavy elements produced by ongoing star formation. Two new quantities enter: $\eta \equiv \frac{(dM/dt)_{OF}}{SFR}$ is the mass outflow rate normalized by the star formation rate, and $\alpha \equiv Z_{OF}/Z_{ISM}$ is the enrichment of the outflow relative to the ambient ISM. For our derivation, we begin with the treatment of Matteucci (2001). We modify equation 5.33 of Matteucci (2001) by adding α to the third term:

$$d(ZM_g)/dt = p SFR - Z SFR - \alpha Z (dM/dt)_{OF}, \quad (\text{A2})$$

where Z is the ISM abundance, M_g is the gas mass, SFR is the star formation rate, and $(dM/dt)_{OF}$ is the mass outflow rate. All quantities but p , η , and α are assumed to be a function of time. Using the fact that $dM_g/dt = -(dM/dt)_{OF} - SFR$ (equation 5.32 of Matteucci 2001), we solve this equation through substitution and integration. The result is the equation for the modified leaky-box case of an outflow with abundance greater than that of the ambient ISM:

$$Z_1(\text{leaky box}, \alpha > 1) = p/c - (M_2/M_1)^{-c/d}(p/c - Z_2), \quad (\text{A3})$$

where $c \equiv \eta(\alpha - 1)$ and $d \equiv \eta + 1$. Because star formation and outflows cannot lower the galaxy's abundance (i.e., $Z_1 \leq Z_2$; see §7), we have the further constraint that $p/c - Z_2 > 0$, or $c \leq p/Z_2$ ($c \leq 2.18$, for our values of p and Z_2). In the case $\alpha = 1$, the proper equation is the standard leaky-box case of an outflow with abundance equal to that of the ambient ISM:

$$Z_1(\text{leaky box}, \alpha = 1) = Z_2 + (p/d) \ln(M_2/M_1). \quad (\text{A4})$$

Rupke et al. (2005c) estimate $\langle \eta \rangle \sim 0.2 - 0.3$ (with a large scatter) for the cool outflow phase of LIRGs and ULIRGs. The cool phase, which is mostly entrained ambient ISM, has $Z_{OF} \sim Z_{ISM}$, or $\alpha = 1$. For star formation plus a cool-gas outflow, $Z_1 = 0.0036 - 0.0039$, which is not far from the closed-box case. Determining η and α for the hot phase of LIRG and ULIRG outflows is quite difficult, as they are poorly constrained observationally. By comparing the mass outflow rate in the cold phase to predictions from starburst models, Rupke et al. (2005c) find η could be as high as ~ 0.1 . Through model fits to the α -element enhancement, X-ray observations suggest α could reach values of ~ 10 (Grimes et al. 2005). These values yield $Z_1 = 0.0045$, 25% lower than the observed abundance. If we combine the hot and cold phases, we have $\eta \sim 0.3 - 0.4$ and $\langle \alpha \rangle \sim 4 - 4.3$, which yields $Z_1 = 0.0046 - 0.0051$. This is only 15 – 20% lower than the average observed abundance in LIRGs and ULIRGs.

This exercise, though difficult because of observational uncertainties, demonstrates two things: (a) the amount of post-inflow enrichment required to reach the observed values of oxygen abundance in LIRGs and ULIRGs need not be large, and (b) galaxy-to-galaxy variations in chemical evolutionary histories following inflow events can easily produce part of the observed scatter in abundances (through, e.g., varying degrees of gas consumption, outflow enrichment, and outflow efficiency).

REFERENCES

Adelman-McCarthy, J. K., et al. 2006, *ApJS*, 162, 38
 Adelman-McCarthy, J. K., et al. 2007, arXiv:0707.3380 [astro-ph]
 Armus, L., et al. 2007, *ApJ*, 656, 148
 Arribas, S., Bushouse, H., Lucas, R. A., Colina, L., & Borne, K. D. 2004, *AJ*, 127, 2522
 Asplund, M., Grevesse, N., Sauval, A. J., Allende Prieto, C., & Kiselman, D. 2004, *A&A*, 417, 751
 Barnes, J. E., & Hernquist, L. 1996, *ApJ*, 471, 115
 Barton, E. J., Geller, M. J., & Kenyon, S. J. 2000, *ApJ*, 530, 660
 Bell, E. F., & de Jong, R. S. 2000, *MNRAS*, 312, 497
 Bresolin, F. 2007, *ApJ*, 656, 186
 Bresolin, F., Schaerer, D., González Delgado, R. M., & Stasińska, G. 2005, *A&A*, 441, 981
 Bridge, C. R., et al. 2007, *ApJ*, 659, 931
 Brooks, A. M., Governati, F., Booth, C. M., Willman, B., Gardner, J. P., Wadsley, J., Stinson, G., & Quinn, T. 2007, *ApJ*, 655, L17
 Calzetti, D., Armus, L., Bohlin, R. C., Kinney, A. L., Koornneef, J., & Storchi-Bergmann, T. 2000, *ApJ*, 533, 682
 Caputi, K. I., et al. 2007, *ApJ*, 660, 97
 Carico, D. P., Sanders, D. B., Soifer, B. T., Matthews, K., & Neugebauer, G. 1990, *AJ*, 100, 70
 Chapman, S. C., Blain, A. W., Smail, I., & Ivison, R. J. 2005, *ApJ*, 622, 772
 Charlot, S., & Longhetti, M. 2001, *MNRAS*, 323, 887
 Clements, D. L., Desert, F.-X., & Franceschini, A. 2001, *MNRAS*, 325, 665
 Cutri, R. M., et al. 2006, Explanatory Supplement to the 2MASS All Sky Data Release and Extended Mission Products (Pasadena: IPAC), <http://www.ipac.caltech.edu/2mass/releases/allsky/doc/explsup.html>
 Daddi, E., et al. 2005, *ApJ*, 631, L13
 Dalcanton, J. J. 2007, *ApJ*, 658, 941
 Dasyra, K. M., et al. 2006a, *ApJ*, 638, 745
 Dasyra, K. M., et al. 2007, *ApJ*, 657, 102
 Dasyra, K. M., et al. 2006b, *ApJ*, 651, 835
 Davies, R. I., Burston, A., & Ward, M. J. 2002, *MNRAS*, 329, 367
 Dopita, M. A., & Sutherland, R. S. 1995, *ApJ*, 455, 468
 Downes, D., & Solomon, P. M. 1998, *ApJ*, 507, 615
 Draine, B. T. 2003, *ARA&A*, 41, 241
 Edmunds, M. G. 1990, *MNRAS*, 246, 678
 Edmunds, M. G., & Greenhow, R. M. 1995, *MNRAS*, 272, 241
 Edmunds, M. G., & Pagel, B. E. J. 1984, *MNRAS*, 211, 507
 Erb, D. K., Shapley, A. E., Pettini, M., Steidel, C. C., Reddy, N. A., & Adelberger, K. L. 2006, *ApJ*, 644, 813
 Falco, E. E., et al. 1999, *PASP*, 111, 438
 Farrah, D., Afonso, J., Efstathiou, A., Rowan-Robinson, M., Fox, M., & Clements, D. 2003, *MNRAS*, 343, 585
 Genzel, R., et al. 1998, *ApJ*, 498, 579
 Genzel, R., Tacconi, L. J., Rigopoulou, D., Lutz, D., & Tecza, M. 2001, *ApJ*, 563, 527
 Greve, T. R., et al. 2005, *MNRAS*, 359, 1165
 Grimes, J. P., Heckman, T., Strickland, D., & Ptak, A. 2005, *ApJ*, 628, 187
 Hammer, F., et al. 1997, *ApJ*, 481, 49
 Hao, L., Weedman, D. W., Spoon, H. W. W., Marshall, J. A., Levenson, N. A., Elitzur, M., & Houck, J. R. 2007, *ApJ*, 655, L77
 Hartwick, F. D. A. 1976, *ApJ*, 209, 418
 Heckman, T. M., Lehnert, M. D., Strickland, D. K., & Armus, L. 2000, *ApJS*, 129, 493
 Hummer, D. G., & Storey, P. J. 1987, *MNRAS*, 224, 801
 Iono, D., Yun, M. S., & Mihos, J. C. 2004, *ApJ*, 616, 199
 Ishida, C. M. 2004, Ph.D. Thesis
 Jarrett, T. H., Chester, T., Cutri, R., Schneider, S. E., & Huchra, J. P. 2003, *AJ*, 125, 525
 Kauffmann, G., et al. 2003, *MNRAS*, 346, 1055
 Kennicutt, Jr., R. C., Bresolin, F., & Garnett, D. R. 2003, *ApJ*, 591, 801
 Kewley, L. J., & Dopita, M. A. 2002, *ApJS*, 142, 35
 Kewley, L. J., Dopita, M. A., Sutherland, R. S., Heisler, C. A., & Trevena, J. 2001, *ApJ*, 556, 121
 Kewley, L. J., Geller, M. J., & Barton, E. J. 2006a, *AJ*, 131, 2004
 Kewley, L. J., Groves, B., Kauffmann, G., & Heckman, T. 2006b, *MNRAS*, 372, 961
 Kewley, L. J., Jansen, R. A., & Geller, M. J. 2005, *PASP*, 117, 227
 Kim, D.-C., & Sanders, D. B. 1998, *ApJS*, 119, 41
 Kim, D.-C., Sanders, D. B., Veilleux, S., Mazzarella, J. M., & Soifer, B. T. 1995, *ApJS*, 98, 129
 Kim, D.-C., Veilleux, S., & Sanders, D. B. 1998, *ApJ*, 508, 627
 —, 2002, *ApJS*, 143, 277
 Kobulnicky, H. A., & Kewley, L. J. 2004, *ApJ*, 617, 240
 Köppen, J., & Edmunds, M. G. 1999, *MNRAS*, 306, 317
 Köppen, J., Weidner, C., & Kroupa, P. 2007, *MNRAS*, 1479
 Kuzio de Naray, R., McGaugh, S. S., & de Blok, W. J. G. 2004, *MNRAS*, 355, 887
 Le Floc'h, E., et al. 2005, *ApJ*, 632, 169
 Leitherer, C., et al. 1999, *ApJS*, 123, 3
 Liang, Y. C., Hammer, F., & Flores, H. 2006, *A&A*, 447, 113
 Liang, Y. C., Hammer, F., Flores, H., Elbaz, D., Marcillac, D., & Cesarsky, C. J. 2004, *A&A*, 423, 867
 Lilly, S. J., Carollo, C. M., & Stockton, A. N. 2003, *ApJ*, 597, 730
 Liu, C. T., & Kennicutt, Jr., R. C. 1995, *ApJ*, 450, 547
 Lonsdale, C. J., Farrah, D., & Smith, H. E. 2006, Ultraluminous Infrared Galaxies (Astrophysics Update 2), 285
 Lutz, D., Veilleux, S., & Genzel, R. 1999, *ApJ*, 517, L13
 Madau, P., Pozzetti, L., & Dickinson, M. 1998, *ApJ*, 498, 106

Maier, C., Lilly, S. J., Carollo, C. M., Stockton, A., & Brodwin, M. 2005, *ApJ*, 634, 849

Martin, C. L. 2005, *ApJ*, 621, 227

—. 2006, *ApJ*, 647, 222

Matteucci, F. 2001, The Chemical Evolution of the Galaxy (Astrophysics and Space Science Library, Vol. 253; Dordrecht: Kluwer)

McGaugh, S. S. 1991, *ApJ*, 380, 140

Melbourne, J., Koo, D. C., & Le Floc'h, E. 2005, *ApJ*, 632, L65

Menzel, D. H. 1969, *ApJS*, 18, 221

Mihos, J. C., & Hernquist, L. 1996, *ApJ*, 464, 641

Miller, J. S., & Mathews, W. G. 1972, *ApJ*, 172, 593

Mirabel, I. F., & Sanders, D. B. 1988, *ApJ*, 335, 104

—. 1989, *ApJ*, 340, L53

Mouhcine, M., Bamford, S. P., Aragón-Salamanca, A., Nakamura, O., & Milvang-Jensen, B. 2006, *MNRAS*, 369, 891

Moustakas, J., & Kennicutt, Jr., R. C. 2006, *ApJS*, 164, 81

Naab, T., Jesseit, R., & Burkert, A. 2006, *MNRAS*, 372, 839

Nesvadba, N. P. H., et al. 2007, *ApJ*, 657, 725

Pasquali, A., Kauffmann, G., & Heckman, T. M. 2005, *MNRAS*, 361, 1121

Patris, J., Dennefeld, M., Lagache, G., & Dole, H. 2003, *A&A*, 412, 349

Pilyugin, L. S., & Thuan, T. X. 2005, *ApJ*, 631, 231

Reddy, N. A., Steidel, C. C., Fadda, D., Yan, L., Pettini, M., Shapley, A. E., Erb, D. K., & Adelberger, K. L. 2006, *ApJ*, 644, 792

Rothberg, B., & Joseph, R. D. 2006, *AJ*, 132, 976

Rupke, D. S., Veilleux, S., & Sanders, D. B. 2002, *ApJ*, 570, 588

—. 2005a, *ApJ*, 632, 751

—. 2005b, *ApJS*, 160, 87

—. 2005c, *ApJS*, 160, 115

Salzer, J. J., et al. 2000, *AJ*, 120, 80

Salzer, J. J., Lee, J. C., Melbourne, J., Hinz, J. L., Alonso-Herrero, A., & Jangren, A. 2005, *ApJ*, 624, 661

Sanders, D. B., Mazzarella, J. M., Kim, D.-C., Surace, J. A., & Soifer, B. T. 2003, *AJ*, 126, 1607

Sanders, D. B., & Mirabel, I. F. 1996, *ARA&A*, 34, 749

Sanders, D. B., Scoville, N. Z., & Soifer, B. T. 1991, *ApJ*, 370, 158

Sanders, D. B., Soifer, B. T., Elias, J. H., Madore, B. F., Matthews, K., Neugebauer, G., & Scoville, N. Z. 1988, *ApJ*, 325, 74

Savaglio, S., et al. 2005, *ApJ*, 635, 260

Schmidt, M., Schneider, D. P., & Gunn, J. E. 1995, *AJ*, 110, 68

Scoville, N. Z., et al. L. 2000, *AJ*, 119, 991

Shi, Y., Rieke, G. H., Papovich, C., Pérez-González, P. G., & Le Floc'h, E. 2006, *ApJ*, 645, 199

Smail, I., Chapman, S. C., Blain, A. W., & Ivison, R. J. 2004, *ApJ*, 616, 71

Stanford, S. A., Stern, D., van Breugel, W., & De Breuck, C. 2000, *ApJS*, 131, 185

Strauss, M. A., Huchra, J. P., Davis, M., Yahil, A., Fisher, K. B., & Tonry, J. 1992, *ApJS*, 83, 29

Strauss, M. A., et al. 2002, *AJ*, 124, 1810

Surace, J. A., Sanders, D. B., & Evans, A. S. 2000, *ApJ*, 529, 170

Surace, J. A., Sanders, D. B., & Mazzarella, J. M. 2004, *AJ*, 127, 3235

Swinbank, A. M., Smail, I., Chapman, S. C., Blain, A. W., Ivison, R. J., & Keel, W. C. 2004, *ApJ*, 617, 64

Tacconi, L. J., Genzel, R., Lutz, D., Rigopoulou, D., Baker, A. J., Iserlohe, C., & Tecza, M. 2002, *ApJ*, 580, 73

Tacconi, L. J., et al. 2006, *ApJ*, 640, 228

Talbot, Jr., R. J., & Arnett, W. D. 1971, *ApJ*, 170, 409

Tecza, M., et al. 2004, *ApJ*, 605, L109

Thronson, Jr., H. A., Majewski, S., Descartes, L., & Hereld, M. 1990, *ApJ*, 364, 456

Tokunaga, A. T., & Vacca, W. D. 2005, *PASP*, 117, 421

Tremonti, C. A., et al. 2004, *ApJ*, 613, 898

Trentham, N., Kormendy, J., & Sanders, D. B. 1999, *AJ*, 117, 2152

van Zee, L., Salzer, J. J., & Haynes, M. P. 1998, *ApJ*, 497, L1

Veilleux, S., Cecil, G., & Bland-Hawthorn, J. 2005, *ARA&A*, 43, 769

Veilleux, S., et al. 2006, *ApJ*, 643, 707

Veilleux, S., Kim, D.-C., & Sanders, D. B. 1999, *ApJ*, 522, 113

—. 2002, *ApJS*, 143, 315

Veilleux, S., Kim, D.-C., Sanders, D. B., Mazzarella, J. M., & Soifer, B. T. 1995, *ApJS*, 98, 171

Veilleux, S., & Osterbrock, D. E. 1987, *ApJS*, 63, 295

Wainscoat, R. J., & Cowie, L. L. 1992, *AJ*, 103, 332

Wang, W.-H., Cowie, L. L., & Barger, A. J. 2006, *ApJ*, 647, 74

Wu, H., Zou, Z. L., Xia, X. Y., & Deng, Z. G. 1998, *A&AS*, 132, 181

York, D. G., et al. 2000, *AJ*, 120, 1579

Zaritsky, D., Kennicutt, Jr., R. C., & Huchra, J. P. 1994, *ApJ*, 420, 87

TABLE 1
SAMPLE

IRAS FSC (1)	Nuclear ID (2)	Redshift (3)	L_{IR} (4)	K_s (5)	% Lum. (6)	Sample (7)	Ref (8)
LIRGs							
F00189+3748	2MASX J00213417+3805347	0.036	11.34	-25.06	100.00	2jy	3
F00267+3016:NW	2MASXi J0029256+303325	0.050	11.73	-25.39	76.80	2jy	3
F00267+3016:SE	2MASX J00292498+3033339	0.050	11.21	-24.09	23.19	2jy	3
F01173+1405	2MASX J01200265+1421417	0.0312	11.63	-24.38	100.00	rbgs	423
F01364-1042	2MASX J01385289-1027113	0.0484	11.76	-23.88	100.00	rbgs	4
F01484+2220	2MASX J01511437+2234561	0.0323	11.64	-25.50	100.00	rbgs	5
F02248+2621	2MASX J02274641+2635222	0.033	11.42	-24.59	100.00	2jy	3
F02512+1446	UGC 2369 NED01 ^a	0.0315	11.70	-24.36	100.00	rbgs	31
F1_5	[CDF99] F1_005	0.4786	11.85	-1.00	100.00	cdf	1
F04315-0840	2MASX J04340002-0834445	0.0160	11.60	-24.74	100.00	rbgs	6
F06538+4628:SW	2MASX J06573445+4624108	0.021	11.31	-24.03	100.00	rbgs	3
IRAS07062+2041	2MASX J07091189+2036102	0.017	11.13	-24.17	100.00	2jy	3
IRAS07063+2043	2MASX J07091808+2038092	0.017	11.26	-24.80	100.00	rbgs	3
F07256+3355	2MASX J07285341+3349084	0.013	11.23	-24.16	100.00	rbgs	3
F08572+3915:SE	IRAS 08572+3915NW	0.0583	11.23	-22.17	13.57	1jy	4
F09046+1838	2MASX J09073082+1826057	0.029	11.31	-24.78	100.00	2jy	3
F09126+4432:NE	2MASX J09155548+4419576	0.0398	11.70	-25.28	100.00	rbgs	4
F09209+3943:E	2MASX J09240034+3930426	0.0921	11.52	-25.17	65.29	wgs	24
F09209+3943:W	2MASX J09235974+3930456	0.0922	11.25	-24.49	34.70	wgs	4
F09218+3428	FIRST J092455.0+341535	0.068	11.72	-1.00	100.00	wgs	2
F09320+6134	2MASX J09355169+6121105	0.0393	11.96	-25.53	100.00	rbgs	423
F09333+4841	2MASX J09363719+4828275	0.0259	11.37	-24.20	100.00	rbgs	3
F09338+3133	2MASX J09364832+3119507	0.077	11.62	-24.86	100.00	wgs	2
F09339+2835	2MASX J09365478+2822200	0.119	11.78	-24.96	100.00	wgs	2
F09399+2830	2MASX J09425370+2816563	0.053	11.17	-23.58	100.00	wgs	2
F10190+1322:W	F10190+1322W	0.0766	11.68	-24.93	41.56	1jy	1
F10190+1322:E	F10190+1322E	0.0759	11.82	-25.27	58.44	1jy	41
F10203+5235	2MASX J10233258+5220308	0.0322	11.43	-24.94	100.00	2jy	34
F10594+3818:SW	F10594+3818SW	0.1578	11.94	-24.68	38.03	1jy	4
F11231+1456	2MASX J11254505+1440359	0.034	11.57	-24.81	100.00	rbgs	3
F12116+5448	2MASX J12140957+5431360	0.0081	11.06	-23.09	100.00	rbgs	64
F12251+4026	2MASX J12273800+4009378	0.037	11.49	-24.72	100.00	2jy	3
F12592+0436	2MASX J13015026+0420005	0.0373	11.62	-24.84	100.00	rbgs	4
F13136+6223	2MASX J13153506+6207287	0.031	11.79	-24.18	100.00	rbgs	4236
F13182+3424	2MASX J13203537+3408218	0.022	11.67	-23.98	100.00	rbgs	56
F13373+0105:NW	2MASX J13395227+0050224	0.022	11.39	-24.82	100.00	rbgs	6
F13373+0105:SE	2MASX J13395767+0049514	0.023	11.15	-25.04	100.00	rbgs	6
F13458+1540:NE	2MASX J13481477+1525497	0.058	11.43	-24.96	49.07	2jy	3
F13458+1540:SW	CGCG 102-061 NED01 ^a	0.058	11.45	-25.00	50.92	2jy	3
F14179+4927	2MASX J14194323+4914121	0.026	11.32	-23.97	100.00	rbgs	5
F14280+3126	2MASX J14301041+3112558	0.012	11.06	-24.40	100.00	rbgs	5
F14416+6618	2MASX J14423488+6606043	0.038	11.27	-23.38	100.00	wgs	2
F15043+5754:S	F15043+5754S	0.1505	11.94	-25.44	49.54	1jy	4
F15163+4255:NW	2MASX J15180612+4244445	0.039	11.90	-24.63	100.00	rbgs	5
F15359+3139	2MASX J15375657+3129582	0.0534	11.02	-23.82	100.00	wgs	24
F15384+3841	2MASX J15401502+3832111	0.0673	11.24	-24.82	100.00	wgs	24
F15386+3807	FIRST J154031.0+375814	0.1828	11.62	-1.00	100.00	ff	1
F15391+3214:SE	2MASX J15410590+3204466	0.0530	11.39	-24.06	100.00	wgs	24
F15394+3532	F15394+3532	0.1235	11.81	-1.00	100.00	wgs	24
F15519+3537	2MASX J15534897+3528042	0.0842	11.66	-25.54	100.00	wgs	24
F15543+3013	FIRST J155623.3+300443	0.121	11.71	-1.00	100.00	wgs	2
F15543+4158:NW	2MASX J15560483+4149304	0.134	11.74	-25.55	74.96	wgs	2
F15543+4158:SE	FIRST J155605.3+414922	0.1342	11.26	-24.53	25.03	wgs	24
F15549+4201	2MASX J15563641+4152501	0.0348	11.16	-24.30	100.00	wgs	24
F16030+2040	2MASX J16051287+2032326	0.015	11.02	-23.38	100.00	rbgs	5
F16104+5235:NE	2MASX J16114086+5227270	0.0295	11.51	-24.70	100.00	rbgs	54
F16333+4630:E	F16333+4630E	0.1908	11.36	-23.20	7.49	1jy	1
F16474+3430:N	F16474+3430N	0.1126	11.43	-23.82	15.28	1jy	4
F16504+0228	2MASX J16525886+0224035	0.0243	11.86	-26.02	100.00	rbgs	5
F16577+5900:SE	2MASX J16583138+5856102	0.019	11.26	-24.82	100.00	rbgs	5
F18131+6820	2MASX J18125527+6821484	0.020	11.23	-24.83	100.00	rbgs	6
F18425+6036	2MASX J18431242+6039121	0.013	11.06	-24.45	100.00	rbgs	5
F20550+1655:SE	2MASX J2057240+170735	0.035	11.88	-23.36	100.00	rbgs	3
F22204-0214:NW	2MASX J22225728-0159290	0.139	11.94	-24.30	57.27	wgs	2
F22204-0214:SE	...	0.140	11.82	-23.99	42.72	wgs	2
F23488+2018	2MASX J23511863+2034404	0.018	11.53	-24.58	100.00	rbgs	3
ULIRGs							
F01298-0744	F01298-0744	0.1361	12.41	-24.38	100.00	1jy	1
F03250+1606	F03250+1606	0.1290	12.19	-25.93	100.00	1jy	1
F04313-1649	F04313-1649	0.2672	12.72	-25.14	100.00	1jy	1

TABLE 1 — *Continued*

<i>IRAS</i> FSC (1)	Nuclear ID (2)	Redshift (3)	L_{IR} (4)	K_s (5)	% Lum. (6)	Sample (7)	Ref (8)
F08136+3110	FIRST J081645.7+310119	0.4070	12.46	-26.30	100.00	ff	1
F08201+2801	F08201+2801	0.1678	12.37	-25.28	100.00	1jy	4
F08208+3211	FIRST J082354.6+320212	0.3955	12.49	-25.83	100.00	ff	1
F08474+1813	F08474+1813	0.1454	12.28	-24.18	100.00	1jy	1
F08572+3915:NW	IRAS 08572+3915NW	0.058	12.04	-24.09	86.43	1jy	46
F08591+5248	F08591+5248	0.1573	12.30	-26.03	100.00	1jy	4
F09039+0503	F09039+0503	0.1252	12.16	-25.18	100.00	1jy	14
F09116+0334:W	F09116+0334W	0.1454	12.22	-26.35	94.61	1jy	14
F09245+3300	FIRST J092734.7+324713	0.222	12.30	-1.00	100.00	wgs	2
F09539+0857	F09539+0857	0.1290	12.19	-24.37	100.00	1jy	1
F10091+4704	F10091+4704	0.2451	12.70	-25.96	100.00	1jy	1
F10156+3705	FIRST J101834.5+364951	0.4895	12.82	-26.08	100.00	ff	1
F10494+4424	F10494+4424	0.0919	12.23	-25.05	100.00	1jy	4
F10565+2448	2MASX J10591815+2432343	0.0430	12.04	-25.03	100.00	rbgs	3
F11028+3130	F11028+3130	0.1986	12.49	-24.65	100.00	1jy	4
F11387+4116	F11387+4116	0.1489	12.26	-25.50	100.00	1jy	14
F11506+1331	F11506+1331	0.1274	12.39	-25.39	100.00	1jy	4
F12112+0305:NE	F12112+0305NE	0.073	12.00	-24.21	45.64	1jy	436
F12112+0305:SW	F12112+0305SW	0.0730	12.08	-24.40	54.36	1jy	43
F13469+5833:W	F13469+5833W	0.1575	12.04	-24.64	59.11	1jy	4
F14348-1447:SW	F14348-1447SW	0.083	12.15	-25.18	62.18	1jy	6
F15206+3342	F15206+3342	0.1254	12.26	-25.61	100.00	1jy	42
F15250+3608	2MASX J15265942+3558372	0.0552	12.02	-24.27	100.00	rbgs	46
F15414+3238	FIRST J154326.4+322859	0.2033	12.12	-1.00	100.00	wgs	24
F16007+3743	2MASX J16023279+3734532	0.185	12.09	-26.18	100.00	wgs	2
F16333+4630:W	F16333+4630W	0.1908	12.45	-25.85	92.51	1jy	1
F17068+4027:E	F17068+4027E	0.1794	12.34	-25.31	78.04	1jy	1
F22381-1337	2MASX J22404826-1321360	0.110	12.02	-24.64	100.00	wgs	2
F22491-1808	F22491-1808	0.076	12.17	-24.92	100.00	1jy	26
F23234+0946:W	F23234+0946W	0.1279	12.07	-25.41	78.72	1jy	1
F23365+3604	2MASX J23390127+3621087	0.065	12.13	-25.22	100.00	rbgs	2

REFERENCES. — 1 = Rupke et al. (2002, 2005b); 2 = Kim et al. (1995); 3 = Wu et al. (1998); 4 = SDSS; 5 = Moustakas & Kennicutt (2006); 6 = Liu & Kennicutt (1995)

NOTE. — Col.(1): Galaxy nucleus designation from the *IRAS* Faint Source Catalog. Two sources are *IRAS* sources but not in the FSC, and a third is not an *IRAS* source (F1.5; Clements et al. 2001). The nucleus is specified if the *IRAS* flux is unresolved or spread among two or more nuclei. Col.(2): Designation, in NED nomenclature, which precisely specifies in sky coordinates the galaxy nucleus from which the *IRAS* flux and spectrum originate. For 1 Jy ULIRGs, the nuclei are already known (Kim et al. 2002; Veilleux et al. 2002). For non-1 Jy ULIRGs and all LIRGs, we specify a unique galaxy nucleus designation. 2MASS sources are used where possible. Col.(3): Redshift. Sources are, in order of preference, the SDSS, Rupke et al. (2005b), Kim et al. (1995), Wu et al. (1998), or NED. Col.(4): Redshift. Sources are, in order of preference, the SDSS, Rupke et al. (2005b), Kim et al. (1995), Wu et al. (1998), or NED. Col.(5): K_s -band absolute magnitude, compiled and computed as described in §4.1. Col.(6): Fraction of (unresolved) total infrared luminosity originating in this nucleus, based on K -band flux ratios for individual nuclei. Col.(7): Sample from which galaxy is taken: rbgs = Revised Bright Galaxy Sample (Sanders et al. 2003), 1jy = the 1 Jy sample (Kim & Sanders 1998), wgs = Warm Galaxy Sample (Kim et al. 1995), 2jy = the 2 Jy sample (Strauss et al. 1992), and ff = the FIRST/FSC sample (Stanford et al. 2000). Col.(8): Spectrum reference; the first reference is the data we use in our analysis.

^a A 2MASS designation exists for this galaxy, but it is attached to another nucleus.

TABLE 2
NEW LINE FLUXES

IRAS FSC	E($B-V$)	W_{eq}^{em} (H α)	W_{eq}^{abs} (H β)	[O II]	H β	[O III]	[O I]	H α	[N II]	[S II]	[S II]
				3726+3729	4861	5007	6300	6563	6583	6716	6731
(1)	(2)	(3)	(4)	(5)	(6)	(7)	(8)	(9)	(10)	(11)	(12)
LIRGs											
F01173+1405	0.93	-202.00	3.29	9.83e-15	7.17e-15	6.67e-15	2.73e-15	6.02e-14	2.50e-14	1.05e-14	8.90e-15
F01364-1042	1.28	-18.30	9.84	1.83e-15	3.63e-16	3.94e-16	7.32e-16	3.19e-15	3.08e-15	1.27e-15	9.90e-16
F1_5	0.91	-119.48	6.13	1.49e-16	1.43e-16	5.56e-17	...	1.14e-15	5.13e-16	1.86e-16	...
F08572+3915:SE	0.44	-45.39	4.02	1.66e-15	8.70e-16	4.80e-16	1.20e-16	3.89e-15	1.15e-15	7.87e-16	5.89e-16
F09126+4432:NE	1.45	-14.40	8.72	1.83e-15	6.29e-16	3.62e-16	3.80e-16	6.53e-15	6.14e-15	1.47e-15	1.07e-15
F09209+3943:W	1.07	-11.03	5.10	8.19e-16	2.00e-16	2.09e-16	...	1.45e-15	9.87e-16	4.85e-16	3.52e-16
F09320+6134	1.63	-35.72	9.80	1.95e-15	1.02e-15	1.67e-15	1.07e-15	1.60e-14	1.92e-14	3.34e-15	2.53e-15
F10190+1322:W	0.89	-36.10	6.14	9.21e-16	1.31e-15	2.16e-16	2.35e-16	9.31e-15	5.47e-15	1.08e-15	9.88e-16
F10190+1322:E	1.88	-18.90	10.17	5.05e-16	1.57e-16	1.86e-16	3.43e-16	2.80e-15	2.41e-15	6.55e-16	4.80e-16
F10594+3818:SW	0.51	-98.90	9.76	4.48e-15	3.10e-15	1.60e-15	6.97e-16	1.49e-14	7.74e-15	2.62e-15	2.05e-15
F12592+0436	1.34	-17.02	9.03	1.25e-15	4.46e-16	3.81e-16	5.46e-16	4.24e-15	3.63e-15
F13136+6223	0.63	-244.90	4.24	5.57e-14	3.00e-14	3.51e-14	5.64e-15	1.78e-13	6.93e-14	2.27e-14	2.10e-14
F15043+5754:S	0.52	-80.16	5.82	2.36e-15	1.27e-15	7.97e-16	2.58e-16	6.28e-15	8.18e-16	1.18e-15	9.12e-16
F15386+3807	1.21	-75.33	4.84	1.56e-16	9.91e-17	8.59e-17	4.70e-17	1.11e-15	7.54e-16	2.00e-16	1.56e-16
F16333+4630:E	0.49	-54.53	5.42	2.10e-16	9.50e-17	8.71e-17	2.50e-17	4.47e-16	1.73e-16	8.70e-17	6.31e-17
F16474+3430:N	0.57	-66.99	7.80	2.12e-15	1.02e-15	6.19e-16	1.70e-16	5.20e-15	7.02e-16	9.81e-16	7.10e-16
ULIRGs											
F01298-0744	0.92	-39.24	3.60	4.14e-16	2.26e-16	2.33e-16	1.80e-16	1.76e-15	9.46e-16
F03250+1606	0.90	-23.10	6.95	7.92e-16	5.54e-16	5.65e-16	5.69e-16	3.61e-15	3.64e-15
F04313-1649	1.66	-38.68	8.67	3.84e-16	2.23e-16	1.85e-16	1.22e-16	3.75e-15	9.30e-16	3.54e-16	2.71e-16
F08136+3110	0.75	-118.41	6.72	5.90e-16	1.88e-16	2.10e-16	1.35e-16	1.23e-15	5.92e-16	3.40e-16	2.00e-16
F08201+2801	0.81	-80.65	7.71	1.88e-15	8.30e-16	6.51e-16	3.07e-16	5.71e-15	2.49e-15	1.06e-15	8.60e-16
F08208+3211	0.79	-95.11	2.69	2.67e-16	1.25e-16	1.41e-16	4.80e-17	8.83e-16	4.74e-16	...	1.42e-16
F08474+1813	1.56	-11.77	6.75	1.57e-16	3.30e-17	6.39e-17	5.15e-17	3.94e-16	5.44e-16	1.30e-16	1.09e-16
F08572+3915:NW	0.69	-59.57	7.00	2.09e-15	1.25e-15	1.12e-15	4.60e-16	7.29e-15	2.89e-15	1.85e-15	1.35e-15
F08591+5248	0.82	-42.95	9.49	1.96e-15	9.42e-16	4.55e-16	4.32e-16	5.91e-15	4.40e-15	1.22e-15	9.98e-16
F09039+0503	0.54	-85.37	8.88	2.75e-15	2.07e-15	1.15e-15	1.03e-15	1.03e-14	7.52e-15	2.68e-15	2.56e-15
F09116+0334:W	1.06	-25.11	11.69	2.30e-15	1.00e-15	5.46e-16	6.82e-16	7.15e-15	7.50e-15	...	1.35e-15
F09539+0857	0.97	-33.12	9.30	1.82e-15	3.19e-16	6.69e-16	4.88e-16	2.30e-15	3.65e-15	9.83e-16	...
F10091+4704	1.09	-25.28	5.86	2.87e-16	6.95e-17	8.72e-17	1.06e-16	6.00e-16	6.24e-16	2.68e-16	1.94e-16
F10156+3705	0.21	-229.17	8.46	7.44e-16	2.56e-16	3.75e-16	...	9.08e-16	3.50e-16	...	1.30e-16
F10494+4424	1.43	-50.70	7.00	8.37e-16	3.06e-16	4.72e-16	4.62e-16	4.21e-15	1.07e-15	1.07e-15	8.92e-16
F11028+3130	-0.01	-8.44	9.09	4.01e-16	2.82e-16	8.91e-17	...	4.17e-16	3.77e-16	1.90e-16	1.05e-16
F11387+4116	1.02	-27.00	4.34	1.13e-15	4.95e-16	3.10e-16	4.00e-16	4.13e-15	4.10e-15	1.16e-15	1.00e-15
F11506+1331	1.13	-78.60	2.99	1.77e-15	6.16e-16	8.80e-16	5.76e-16	6.41e-15	2.74e-15	1.43e-15	1.13e-15
F12112+0305:NE	0.89	-76.70	8.86	4.63e-15	1.48e-15	2.61e-15	1.07e-15	1.09e-14	4.62e-15	2.74e-15	1.99e-15
F12112+0305:SW	1.33	-38.30	9.17	1.15e-15	3.55e-16	3.82e-16	4.93e-16	4.00e-15	2.60e-15	1.09e-15	8.07e-16
F13469+5833:W	0.98	-26.02	6.44	6.73e-16	3.01e-16	2.17e-16	1.25e-16	2.25e-15	1.86e-15	4.80e-16	3.44e-16
F15206+3342	0.58	-401.00	0.00	3.01e-14	1.93e-14	5.41e-14	3.38e-15	1.09e-13	2.04e-14	9.54e-15	7.87e-15
F15250+3608	0.75	-47.65	5.44	7.03e-15	3.11e-15	3.87e-15	1.49e-15	1.95e-14	9.34e-15	4.13e-15	3.32e-15
F16333+4630:W	0.82	-113.20	6.31	1.13e-15	5.52e-16	8.07e-16	3.58e-16	3.92e-15	2.46e-15	8.72e-16	7.13e-16
F17068+4027:E	0.35	-187.26	11.34	1.25e-15	8.40e-16	1.22e-15	2.21e-16	3.44e-15	1.07e-15	6.70e-16	5.40e-16
F23234+0946:W	0.65	-167.52	0.00	4.00e-15	1.45e-15	1.68e-15	1.02e-15	8.90e-15	9.90e-15	2.66e-15	...

NOTE. — Col.(1): Galaxy designation from the *IRAS* Faint Source Catalog. Col.(2): Optical extinction, measured from the Balmer decrement. Col.(3): H α emission line equivalent width, in Å, uncorrected for underlying absorption. Col.(4): H β stellar absorption line equivalent width. Col.(5-12): Observed line fluxes, in erg s $^{-1}$ cm $^{-2}$. Fluxes are uncorrected for extinction or underlying stellar absorption, except for H β (which has had stellar absorption contamination removed). Line flux measurement errors range are 5% for strong lines, and up to 20 – 30% in a few individual cases for weak lines (e.g., [O I], [O III], and/or [S II]).

TABLE 3
ABUNDANCES

IRAS FSC	log(R ₂₃)	log(O ₃₂)	12-log(O/H)					
			1	2	3	4	5	6
(1)	(2)	(3)	(4)	(5)	(6)	(7)	(8)	(9)
LIRGs								
F00189+3748	0.49	-1.72	8.09	8.82	8.93	9.09	8.95	9.14
F00267+3016:NW	1.36	-1.60
F00267+3016:SE	0.91	-1.01	7.70	8.33	8.44	8.68	8.84	9.10
F01173+1405	0.71	-0.92	8.07	8.63	8.71	8.75	8.88	8.92
F01364-1042	1.37	-1.84
F01484+2220	0.33	-1.10	8.38	8.94	9.04	8.98	9.04	...
F02248+2621	0.34	-0.86	8.45	8.94	9.03	8.91	9.13	9.40
F02512+1446	0.65	-1.14	8.07	8.69	8.79	8.85	8.92	9.07
F1_5	0.54	-1.25	8.16	8.79	8.89	8.92	8.95	9.06
F04315-0840	0.32	-0.15	8.69	8.96	9.05	8.78	9.17	9.31
F06538+4628:SW	0.71	-1.24	7.95	8.61	8.72	8.86	8.88	...
IRAS07062+2041	0.33	-0.78	8.49	8.95	9.04	8.90	9.06	8.97
IRAS07063+2043	0.72	-1.41	7.88	8.58	8.70	8.89	8.94	...
F07256+3355	0.94	-2.06	7.32	8.13	8.39	8.99	8.75	9.27
F08572+3915:SE	0.59	-1.05	8.17	8.75	8.84	8.85	8.84	8.76
F09046+1838	0.76	-1.43	7.81	8.52	8.65	8.87	8.84	9.12
F09126+4432:NE	1.21	-2.02
F09209+3943:E	0.48	-1.27	8.21	8.84	8.94	8.96	8.99	9.09
F09209+3943:W	1.19	-1.59
F09218+3428	0.58	-0.90	8.24	8.77	8.85	8.81	8.95	9.01
F09320+6134	1.16	-1.29
F09333+4841	0.90	-1.24	7.62	8.32	8.45	8.76	8.84	9.13
F09338+3133	0.43	-1.59	8.18	8.87	8.98	9.09	8.99	9.19
F09339+2835	0.56	-1.09	8.19	8.78	8.87	8.87	8.96	9.05
F09399+2830	0.97	-0.94	7.60	8.23	8.34	8.64	8.77	8.97
F10190+1322:W	0.34	-1.51	8.27	8.94	9.04	9.10	9.06	9.36
F10190+1322:E	1.47	-1.97
F10203+5235	0.71	-0.50	8.26	8.66	8.72	8.66	9.01	8.99
F10594+3818:SW	0.51	-0.98	8.28	8.83	8.91	8.87	9.00	9.09
F11231+1456	0.52	-1.77	8.05	8.79	8.90	9.09	8.99	9.32
F12116+5448	0.55	-0.36	8.48	8.82	8.88	8.71	9.04	9.15
F12251+4026	0.59	-1.29	8.09	8.74	8.84	8.92	8.97	...
F12592+0436	1.15	-1.69
F13136+6223	0.73	-0.74	8.13	8.62	8.69	8.70	8.87	9.03
F13182+3424	1.16	-1.52
F13373+0105:NW	0.02	0.17	8.84	9.06	9.18	8.79	9.23	9.45
F13373+0105:SE	0.58	-0.85	8.26	8.77	8.85	8.81	8.67	...
F13458+1540:NE	0.68	-1.23	8.00	8.65	8.75	8.86	8.85	8.96
F13458+1540:SW	0.44	-0.68	8.45	8.89	8.97	8.83	9.04	9.04
F14179+4927	0.31	-1.27	8.35	8.96	9.05	9.03	9.13	...
F14280+3126	0.37	-1.49	8.24	8.92	9.02	9.08	8.99	9.29
F14416+6618	0.77	-0.30	8.27	8.61	8.65	8.59	8.87	8.85
F15043+5754:S	0.62	-1.02	8.15	8.72	8.81	8.83	8.80	8.36
F15163+4255:NW	0.69	-0.87	8.12	8.66	8.74	8.75	8.93	...
F15359+3139	0.90	-1.60	7.51	8.28	8.46	8.86	8.83	9.28
F15384+3841	0.51	-1.09	8.24	8.83	8.92	8.90	8.94	9.37
F15386+3807	0.87	-1.24	7.68	8.37	8.50	8.76	8.88	9.18
F15391+3214:SE	0.71	-1.78	7.81	8.57	8.72	9.01	8.88	9.28
F15394+3532	0.49	-0.84	8.35	8.85	8.93	8.84	8.94	8.95
F15519+3537	0.85	-1.30	7.70	8.41	8.54	8.79	8.84	9.27
F15543+3013	0.59	-0.89	8.23	8.76	8.84	8.80	9.00	9.17
F15543+4158:NW	0.57	-0.69	8.34	8.79	8.87	8.77	8.95	8.72
F15543+4158:SE	0.68	-0.04	8.45	8.72	8.74	8.59	8.87	8.84
F15549+4201	0.76	-0.69	8.10	8.58	8.65	8.68	8.91	9.04
F16030+2040	0.64	-0.78	8.22	8.72	8.79	8.76	8.80	8.68
F16104+5235:NE	0.38	-0.82	8.44	8.92	9.01	8.89	9.06	...
F16333+4630:E	0.71	-0.88	8.10	8.64	8.72	8.75	8.86	8.90
F16474+3430:N	0.68	-1.15
F16504+0228	1.05	-1.28
F16577+5900:SE	0.61	-1.29	8.07	8.73	8.83	8.91	8.95	9.07
F18131+6820	0.23	-0.29	8.69	9.00	9.09	8.85	9.15	9.38
F18425+6036	0.45	-0.97	8.33	8.87	8.96	8.89	9.10	9.23
F20550+1655:SE	0.81	-0.31	8.20	8.55	8.58	8.58	8.74	8.90
F22204-0214:NW	0.98	-1.42	7.36	8.13	8.31	8.77	8.76	9.12
F22204-0214:SE	0.42	-1.31	8.25	8.89	8.98	9.00	9.01	9.40
F23488+2018	0.60	-1.26	8.09	8.74	8.84	8.90	8.97	9.23
ULIRGs								
F01298-0744	0.82	-1.02	7.87	8.48	8.58	8.73	8.86	...
F03250+1606	0.72	-0.86	8.08	8.62	8.70	8.73	9.02	...

TABLE 3 — *Continued*

IRAS FSC	log(R ₂₃)	log(O ₃₂)	12-log(O/H)					
			1	2	3	4	5	6
(1)	(2)	(3)	(4)	(5)	(6)	(7)	(8)	(9)
F04313-1649	1.11	-1.65
F08136+3110	0.95	-1.16	7.55	8.24	8.38	8.71	8.76	8.88
F08201+2801	0.83	-1.22	7.76	8.44	8.56	8.78	8.79	8.97
F08208+3211	0.83	-0.96	7.87	8.47	8.56	8.71	8.87	8.99
F08474+1813	1.49	-1.68
F08572+3915:NW	0.68	-0.87	8.13	8.66	8.74	8.76	8.87	8.75
F08591+5248	0.78	-1.46	7.78	8.50	8.63	8.88	8.91	9.22
F09039+0503	0.51	-0.91	8.31	8.83	8.92	8.85	9.07	9.01
F09116+0334:W	0.93	-1.63	7.43	8.21	8.40	8.86	8.86	9.31
F09245+3300	0.62	-0.86	8.21	8.73	8.81	8.77	8.99	9.13
F09539+0857	1.30	-1.30
F10091+4704	1.21	-1.51
F10156+3705	0.75	-0.56	8.18	8.61	8.66	8.66	8.88	8.88
F10494+4424	1.21	-1.40
F10565+2448	0.91	-1.24	7.60	8.31	8.44	8.75	8.86	9.22
F11028+3130	0.26	-0.87	8.50	8.98	9.08	8.97	9.11	8.99
F11387+4116	0.92	-1.51	7.50	8.26	8.43	8.83	8.91	9.18
F11506+1331	1.09	-1.24
F12112+0305:NE	1.04	-0.99
F12112+0305:SW	1.21	-1.63
F13469+5833:W	0.90	-1.39	7.58	8.31	8.46	8.80	8.87	9.26
F14348-1447:SW	0.57	0.01	8.57	8.82	8.86	8.64	9.12	8.95
F15206+3342	0.82	-0.09	8.28	8.56	8.57	8.44	8.76	8.80
F15250+3608	0.84	-0.90	7.88	8.45	8.54	8.69	8.83	8.92
F15414+3238	0.73	-1.21	7.93	8.58	8.69	8.83	8.92	...
F16007+3743	1.06	-1.46
F16333+4630:W	0.85	-0.80	7.91	8.45	8.53	8.66	8.90	9.01
F17068+4027:E	0.61	-0.27	8.45	8.77	8.82	8.66	8.94	8.70
F22381-1337	0.61	0.01	8.53	8.78	8.82	8.52	8.95	8.82
F22491-1808	0.57	-0.87	8.26	8.78	8.86	8.81	8.96	9.08
F23234+0946:W	0.87	-0.99	7.79	8.41	8.51	8.71	9.01	9.21
F23365+3604	0.64	-1.14	8.08	8.70	8.79	8.85	9.00	9.03

NOTE. — Col.(1): Galaxy designation from the *IRAS* Faint Source Catalog. Col.(2): Logarithm of R₂₃ $\equiv \{f([O\text{ II}]\lambda\lambda 3726, 3729) + f([O\text{ III}]\lambda\lambda 4959, 5007)\}/f(H\beta)$. Col.(2): Logarithm of O₃₂ $\equiv f([O\text{ III}]\lambda\lambda 4959, 5007)/f([O\text{ II}]\lambda\lambda 3726, 3729)$. Col.(4-9): Oxygen abundance from six different diagnostic/calibration systems. 1 = Pilyugin & Thuan 2005; 2 = McGaugh 1991; Kuzio de Naray et al. 2004; 3 = Tremonti et al. 2004; 4 and 6 = Charlot & Longhetti 2001, Cases F and A; and 5 = Kewley & Dopita 2002. See §3.1 for a description of each system.